ENG. Struct. Civ. Eng.
https://doi.org/10.1007/s11709-026-1305-9

RESEARCH ARTICLE

Machine learning-empowered highly efficient seismic fragility estimation of corroded reinforced concrete highway bridge portfolios

Bo XU[a], Xiaowei WANG[b*], Yue LI[a]

[a] *Department of Civil and Environmental Engineering, Case Western Reserve University, Cleveland, OH 44106, USA*
[b] *State Key Laboratory of Disaster Reduction in Civil Engineering, Tongji University, Shanghai 200092, China*
[*] *Corresponding author. E-mail: xiaoweiwang@tongji.edu.cn*

ABSTRACT The seismic fragility of reinforced concrete highway bridges has been found profoundly affected by corrosion-induced degradation. Traditional fragility analysis methods such as the Cloud and Incremental Dynamic Analysis, while effective, they are computationally intensive and impractical for large-scale regional risk and resilience assessments. Additionally, they heavily rely on a predefined probabilistic assumption (i.e., the lognormal distribution in seismic demand and capacity), whose validity remains unknown for corroded structures. To bridge this gap and circumvent this assumption, this study leverages machine learning (ML) to develop a damage-state-classification-driven seismic fragility modeling approach for corroded reinforced concrete bridge portfolios. A comprehensive database is developed through nonlinear time-history analyses, incorporating the effects of bridge structural variability, corrosion levels, and diverse seismic scenarios. Three popular ML classifiers, including artificial neural network (ANN), support vector machine, and *K*-nearest neighbor, are trained and rigorously optimized to map probabilities of damage states directly from structural features and seismic inputs. Analysis results showcase the efficiency and scalability of the ML-empowered method, which significantly reduces computational effort while maintaining well alignment with results from the Cloud method, particularly for the ANN-based one.

KEYWORDS seismic fragility, damage classification, bridge, corrosion, machine learning

1 Introduction

Reinforced concrete (RC) bridges serve as critical infrastructure components of transportation networks, supporting connectivity and economic activities worldwide. However, the progressive aging of these structures poses significant challenges to their seismic resilience, particularly in regions highly prone to earthquakes. Environmental factors, such as chloride-induced corrosion, accelerate the deterioration of steel reinforcement and concrete, exacerbating the seismic vulnerability of RC bridges [1–6]. Corrosion adversely affects mechanical properties of materials, reducing load-carrying capacity and may even altering failure modes of RC components under seismic loading [7–10]. Consequently, accurately and efficiently quantifying seismic fragility of corroded RC bridges is vital for effective risk assessment and resilience planning.

Seismic fragility analyses have been widely used to estimate structural damage probabilities under varying levels of seismic intensities. Traditional methods, such as the Cloud method [11], incremental dynamic analysis (IDA) [12], and multiple stripe analysis (MSA) [13], have been extensively applied within the performance-based earthquake engineering framework (e.g., [14,15], among many others). These approaches typically rely on probabilistic frameworks that use empirical or simulated structural responses, often requiring Monte Carlo simulations and/or extensive nonlinear time-history analysis (NTHA) to derive fragility curves. Apparently, these high computational demands make them impractical for large-scale applications (e.g., network-level bridge

Article history: Received Sep 21, 2025; Accepted Dec 16, 2025

infrastructure assessment). Moreover, a very important assumption in fragility analyses, i.e., the lognormal distribution of seismic demand and capacity, although has been demonstrated for non-corrosive structures [11], is yet to be verified for corroded structures. These limitations hinder the applicability and more importantly the accuracy of conventional methods, particularly for seismic fragility modeling of corroded bridge portfolios toward reliable regional risk assessment.

Advancements in machine learning (ML) offer promising alternatives for seismic fragility analysis by leveraging large data sets to establish complex nonlinear relationships between input features and output predictions. ML-driven approaches provide scalable and efficient solutions for fragility assessment at both individual and regional levels. Early attempts in ML-aided fragility modeling primarily focused on integrating ML regression techniques into probabilistic seismic demand modeling (PSDM) that was often conducted using time-consuming nonlinear finite element (FE) analyses, as demonstrated in past studies on bridges [16] and buildings [17]. However, these methods still rely on the classical assumption that structural demand and capacity follow a lognormal distribution, which may introduce deviations in fragility curve estimations under highly nonlinear scenarios at higher intensity levels [18,19]. Enforcing this lognormal assumption in seismic demand modeling has been shown to result in unrealistic fragility estimates and increased dispersion (i.e., larger lognormal standard deviations) [20]. To overcome the limitations of traditional parametric fragility analyses, non-parametric methods have emerged as viable alternatives. These approaches typically use ML-based regression models to predict seismic demands of structural components, which are then compared against their capacity at specific damage states to generate binary survival-failure vectors. Subsequently, instead of relying on predefined probabilistic distributions, an ML algorithm for classification problems (e.g., the logistic regression as the most popular option) is usually adopted to train an ML model based on these vectors to estimate failure probabilities [21–23]. Unlike traditional PSDMs, which typically rely on a single ground motion intensity measure (IM), the non-parametric approach often incorporates multiple IMs and structural parameters, leading to a more flexible functional representation of fragility.

The most recent studies have increasingly leveraged ML for structural damage classifications, framing fragility assessment as a multi-classification task. In this approach, ML models are trained on labeled data sets to predict the probability of different damage states under varying seismic intensities, and seismic fragility can be subsequently constructed by aggregating exceedance probabilities. Various ML techniques have been explored for post-earthquake damage assessment, such as decision trees and random forest [24,25], artificial neural networks (ANN) [26,27], and support vector machines (SVM) [28,29]. Although these studies highlight the growing role of ML in seismic fragility modeling, their applications in the bridge earthquake engineering domain remain quite limited. Furthermore, existing ML-based fragility analyses just consider pristine structural conditions, while neglecting the impact of deterioration mechanisms like reinforcement corrosion, which may significantly alter seismic fragility in the temporal scale. Addressing these gaps is crucial for developing robust fragility models that account for both aging-related degradation and seismic vulnerability in RC bridge portfolios. After deep investigation of the literature, it is worth mentioning a work by Xu et al. [30], who reported an ML-based life-cycle seismic assessment of corroded RC bridges for post-earthquake damage state predictions, whereas ML-aided seismic fragility models are yet to be established to the best knowledge of the authors.

To fill these gaps remaining in ML-based fragility modeling of corroded RC bridges, particularly at the portfolio level, this study proposes an ML-empowered highly efficient seismic fragility modeling method for corroded RC highway bridge portfolios. The paper is structured as follows. Section 2 introduces the fundamental idea of ML-empowered damage-state-driven method for fragility modeling. Section 3 describes the development of a comprehensive database for corroded RC bridges under seismic loading. Section 4 develops, evaluates, and publicly shares ML models based on three optimized ML algorithms, including ANN, SVM and *K*-nearest neighbors (KNN), for damage classifications. Section 5 showcases and verifies the ML-empowered method via a case study on a specific highway bridge scenario by comparing the ML-derived fragility curves with the well-recognized Cloud method. Finally, a summary of key findings and future research needs are addressed. This study seeks to contribute to the growing body of knowledge on seismic fragility of aging highway bridge infrastructure by demonstrating the feasibility and advantages of ML. The database and trained ML models used in this study are publicly available at Zenodo (DOI: 10.5281/zenodo.17163438) for replication and implementation purposes.

2 Machine learning-empowered damage-state-driven seismic fragility analysis method for corroded bridges

Unlike most existing ML applications in seismic fragility analyses that predominantly focus on regression-based approaches for either demand prediction or capacity estimation, the ML model developed in this study is

designed as a surrogate classifier. It integrates structural attributes, corrosion levels, and seismic IM to predict the probabilities across multiple damage states and identify the most likely state, thereby directly enabling fragility estimates. This classification-based strategy provides a scalable and computationally efficient alternative to conventional simulation-intensive fragility analyses, particularly circumventing the assumption of lognormal distribution in PSDM, thereby facilitating rapid seismic risk assessment across large-scale networks of aging RC bridges. The overall workflow of the proposed method is illustrated in Fig. 1.

For readers less familiar with classification problems, a simple analogy may help. Suppose aiming to identify the breed of a cat, given several possible categories. By observing features such as ear shape, fur type, or tail length, a classifier can assign probabilities to each breed and select the most likely one. The model proposed in this study operates on the same principle: given bridge structural, material, and seismic features, it predicts the probability of each damage state and determines the most likely damage state.

The data set is constructed first by pairing sampled corroded bridge configurations with ground motion records and assigning each pair a discrete damage state label. This process accounts for uncertainties from both corroded bridge conditions and seismic variability. Bridge variability is captured through geometric characteristics, material properties, and reinforcement corrosion levels, while seismic variability is incorporated by a suite of scaled ground motion records with diverse intensities and spectral characteristics. These parameters collectively form the input features, with damage state as the target output. Damage state labels are determined by comparing column drift demands obtained from NTHA against multi-level drift ratio capacity thresholds. These thresholds are derived from a ML-based capacity estimation model, previously proposed by the authors [31], which explicitly incorporates the time-dependent degradation of seismic capacity due to corrosion. This represents a key advantage over traditional approaches which often assume constant capacity or rely on computationally intensive simulations to capture time-dependent deterioration. The numerical modeling for corroded RC bridge under seismic loading is detailed in Section 3. Based on the exceedance of capacity thresholds, each bridge-ground motion pair is categorized into one of five states: none, slight, moderate, extensive, or complete damage.

Multiple ML classification algorithms, such as ANN, SVM, and KNN, are then trained and evaluated on the constructed database. Hyperparameters are optimized via grid search and *k*-fold cross-validation to enhance predictive accuracy and generalization. Model performance is evaluated through metrics such as accuracy, precision, and recall, as detailed in Section 4.

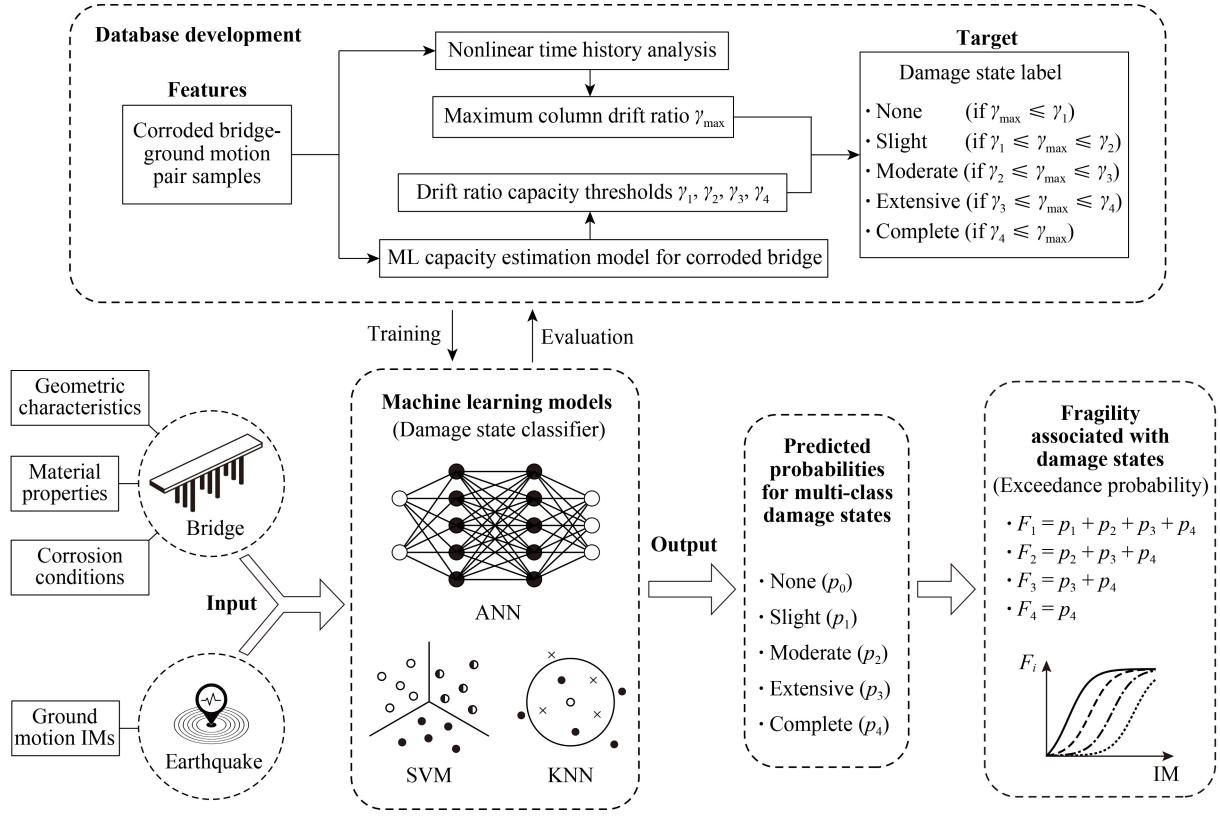

Fig. 1 Workflow of the proposed ML-empowered seismic fragility assessment method for corroded RC bridges.

Once trained, the classifiers can predict the most likely damage state of a corroded bridge subjected to a given earthquake scenario, given input features including bridge geometry, material properties, corrosion levels, and ground motion IMs. More importantly, the classifiers also yield probability distributions across all potential damage states. Fragility at a given damage level is then obtained by summing the predicted probabilities of that state and all more severe states, expressed as

$$F_i = \sum_{k=i}^{4} p_k, \tag{1}$$

where p_k is the predicted probability of damage state k, and F_i is the fragility at damage level i (1 = slight, 2 = moderate, 3 = extensive, 4 = complete).

In contrast to traditional fragility models, the ML method implicitly captures the inherent uncertainties in the demand-capacity relationship through data-driven learning of damage probabilities from a large set of simulated samples. Each training sample represents one realization of the complex interactions among seismic IMs, structural properties, and corrosion conditions, which collectively embody the underlying uncertainties in both seismic demand and structural capacity. Consequently, the resulting fragility curves represent the probabilistic distribution of damage exceedance conditioned on the input features.

3 Development of labeled database for seismic damage states of corroded bridges

As mentioned above, the database is developed through extensive numerical simulations using NTHA. Bridge columns are chosen as the key component in this study, as they are critical load-bearing elements and highly susceptible to seismic damage. Observations from major earthquakes, including the 2008 Wenchuan, 1999 Chi-Chi, and 1995 Hyogo-ken Nanbu earthquakes, have consistently shown that column failure is the predominant failure mode leading to structural instability and bridge collapse [32–34]. Given their role as the most vulnerable components, peak column drift ratio is selected as the primary engineering demand parameter to effectively capture seismic performance and potential failure. By simulating seismic responses of corroded RC bridges across various combinations of structural configurations and seismic intensities, the database captures the intricate interactions among geometric characteristics, material properties, and seismic loading conditions. This section outlines the procedure for the database construction, covering potential bridge parameters, FE modeling, and damage state labeling.

3.1 Bridge structural and ground motion parameters

The seismic performance of corroded RC bridges is influenced by multiple sources of uncertainty, primarily stemming from variations in structural properties, material degradation due to corrosion, and the inherent variability in seismic input. These variations are systematically integrated into the database to ensure realistic and generalizable damage classification across different bridge configurations and seismic scenarios.

Structural parameters are mainly related to geometric characteristics and material properties, both of which significantly affect seismic response. Past studies have consistently shown that variations in span length, column height, and material properties play a crucial role in determining seismic response and should be accounted for in fragility modeling [35]. Sensitivity analyses further highlight that focusing on the most influential parameters, rather than incorporating all possible uncertainties, allows for accurate fragility estimation while maintaining computational efficiency [36]. Additionally, research on bridge classification emphasizes the importance of grouping structures based on key attributes to better capture variability and improve the reliability of fragility predictions [37]. Based on these findings, the parameters in Table 1 are chosen to keep a balance between realistic structural representation and practical feasibility for large-scale seismic risk assessments. These parameters are chosen for their relevance to the seismic performance of corroded RC bridges. Specifically, the number of spans and span length affect the superstructure mass and fundamental period, thereby altering inertial forces and displacement demands. The number, diameter, and height of columns control stiffness, drift capacity, and force distribution, while material properties such as concrete strength and steel yield strength govern stiffness, strength, and energy dissipation. Reinforcement ratios also play a key role: longitudinal reinforcement determines flexural capacity and cracking behavior, whereas transverse reinforcement provides confinement, shear resistance, and ductility. Finally, the axial load ratio captures the interaction between axial and lateral forces, with higher values reducing ductility and increasing collapse risk. Collectively, these parameters represent the essential sources of variability shaping seismic fragility, while keeping the model both realistic and computationally efficient.

Corrosion-related parameters are incorporated by considering the corrosion levels of longitudinal (X_l) and transverse reinforcement (X_t). In this study, X_l is treated as a random variable following a uniform distribution, while X_t is derived as a function of X_l based an empirical ratio $r_{tl} = X_t/X_l$. The ratio r_{tl} is assumed to follow a uniform distribution between 1 and 3, which is intended to adequately cover a wide range of practical degradation

Table 1 Summary of random variables in the corroded RC bridge database

Category	ID	Variable	Name	Distribution	Mean	Std.	Value range	Source (Ref.)
Structure-related (uncorroded)	x_1	N_s	number of spans	discrete uniform	–	–	{2, 3, 4, 5}	–
	x_2	L_s (m)	span length	lognormal	31.775	8.738	[10, 60]	[37]
	x_3	N_c	number of columns per bent	discrete uniform	–	–	{1, 2, 3, 4}	–
	x_4	D (m)	column diameter	uniform	1.525	–	[1.22, 1.83]	[38]
	x_5	H (m)	column height	lognormal	7.133	1.149	[5, 12]	[38]
	x_6	f_c (MPa)	concrete compressive strength	normal	31.37	3.86	[25, 45]	[38]
	x_7	f_y (MPa)	reinforcing steel yield strength	lognormal	465.0	37.3	[300, 600]	[37]
	x_8	ρ_l	column longitudinal reinforcement ratio	uniform	2.00	–	[1.0%, 3.0%]	[38]
	x_9	ρ_t	column transverse reinforcement ratio	uniform	0.85	–	[0.4%, 1.3%]	[38]
	x_{10}	α	axial load ratio	uniform	17.5%	–	[10%, 25%]	–
Corrosion-related	x_{11}	X_l	longitudinal reinforcement corrosion level	uniform	15%	–	[0, 30%]	–
	x_{12}	X_t	transverse reinforcement corrosion level	$X_t = r_{tl}X_l$	–	–	[0, 90%]	–

Note: Std. is the standard deviation, and r_{tl} involving in the definition of X_t is empirical ratio between longitudinal and transverse reinforcement corrosion levels, assumed to follow a uniform distribution between 1 and 3.

scenarios. This reflects the commonly observed phenomenon that transverse reinforcement tends to corrode more rapidly than longitudinal reinforcing steel [39,40], because of their smaller diameters and closer exposure to the concrete surface. This avoids the need for specific time-dependent corrosion models, allowing for flexibility in various applications for different built environments. In other words, instead of prescribing a fixed deterioration model, values of X_l and X_t can be determined based on corrosion models of interest, which ensures adaptability to different environmental and structural conditions for different regions around the world.

In addition to structural and material uncertainties, seismic input variability also significantly affects the seismic performance assessment of corroded RC bridges. Ground motion characteristics inherently exhibit substantial variations in amplitude, frequency content, and duration, which influence structural responses in complex ways. Relying on a single IM has been demonstrated as insufficient for adequately capturing diverse seismic features inherent in earthquake events [27,41]. Consequently, adopting multiple IMs provides a more robust representation of seismic demands, enhancing predictive accuracy in ML-based fragility estimation models [27]. Based on findings from previous studies [27,41–44], this research employs a comprehensive set of 34 IMs to effectively represent seismic input variability and capture diverse ground motion characteristics, thereby facilitating more reliable predictions in ML-empowered seismic damage evaluation models. These IMs are categorized into amplitude-based measures (e.g., peak ground acceleration and peak ground velocity), frequency-based measures (e.g., spectral accelerations at various periods), and duration-based measures (e.g., Arias intensity). A complete list of the IMs, including their definitions and categorizations, is provided in Table 2. It is worth noting that identifying the appropriate IMs for ML modeling is out the scope of this study. The adopted 34 IMs are easy to get via modern computational tools. More importantly, overfitting issues are not detected according to the ML training and test results presented later in this paper.

3.2 Finite element modeling

Three-dimensional (3D) parameterized FE models are developed using the OpenSeesPy (version 3.5.1.12) computational framework [45] to simulate the nonlinear seismic behavior of corroded RC bridges. The model is parameterized, allowing for systematic variation of key inputs such as corrosion levels, material properties, stiffnesses, reinforcement ratios, and geometric dimensions. This parameterization lays the foundation for constructing a comprehensive database under varying seismic intensities, corrosion conditions, and bridge configurations. In this study, corrosion effects are considered only in the bridge columns, as they represent the primary lateral load-resisting components. Other components, including bearings, abutments, and deck connections, are modeled with idealized boundary conditions without considering corrosion-induced degradation. The potential impact of corrosion on these secondary components can be further explored in future system-level extensions of this modeling framework.

As illustrated in Fig. 2, the modeled bridge structure considers a continuous beam bridge system to realistically represent structural continuity and load distribution. The bridge deck is modeled using elastic beam–column elements, as significant damage is not expected to occur in the deck during seismic events. This simplification reduces computational complexity while maintaining the overall accuracy of the bridge model. The

Table 2 Summary of selected IMs

Type	IM	Note	Definition	Unit
Amplitude-based IMs	*PGA*	peak ground acceleration	$\max\|a(t)\|$	g
	PGV	peak ground velocity	$\max\|v(t)\|$	cm/s
	PGD	peak ground displacement	$\max\|d(t)\|$	cm
	ARMS	root-mean-square acceleration	$\sqrt{\frac{1}{SD_{5-95}}\int_{t_{SD5}}^{t_{SD95}}[a(t)]^2\mathrm{d}t}$	g
	VRMS	root-mean-square velocity	$\sqrt{\frac{1}{SD_{5-95}}\int_{t_{SD5}}^{t_{SD95}}[v(t)]^2\mathrm{d}t}$	cm/s
	DRMS	root-mean-square displacement	$\sqrt{\frac{1}{SD_{5-95}}\int_{t_{SD5}}^{t_{SD95}}[d(t)]^2\mathrm{d}t}$	cm
	RVA	peak velocity/acceleration ratio	*PGV*/*PGA*	s
	EDA	effective design acceleration	peak acceleration after filtering frequencies above 9 Hz	g
	SMA	sustained maximum acceleration	Third largest peak in $\|a(t)\|$	g
	SMV	sustained maximum velocity	Third largest peak in $\|v(t)\|$	cm/s
Frequency-based IMs	*ASI*	acceleration spectral intensity	$\int_{0.1}^{0.5} S_\mathrm{a}(T,\,\xi=0.05)\,\mathrm{d}T$	g·s
	VSI	velocity spectrum intensity	$\int_{0.1}^{2.5} S_\mathrm{v}(T,\,\xi=0.05)\,\mathrm{d}T$	cm
	EPA	effective peak acceleration	$\frac{1}{2.5}\mathrm{mean}(S_\mathrm{a}(0.1-0.5,\,\xi=0.05))$	g
	EPV	effective peak velocity	$\frac{1}{2.5}PS_\mathrm{v}(T=1.0,\,\xi=0.05)$	cm/s
	HI	housner intensity	$\int_{0.1}^{2.5} PS_\mathrm{v}(T,\,\xi=0.05)\,dT$	cm
	$S_{\mathrm{a}\text{-}0.2}$	spectral acceleration at 0.2 s	$S_\mathrm{a}(T=0.2,\,\xi=0.05)$	g
	$S_{\mathrm{a}\text{-}1.0}$	spectral acceleration at 1.0 s	$S_\mathrm{a}(T=1.0,\,\xi=0.05)$	g
	$S_{\mathrm{a}\text{-}2.0}$	spectral acceleration at 2.0 s	$S_\mathrm{a}(T=2.0,\,\xi=0.05)$	g
	$S_{\mathrm{v}\text{-}0.2}$	spectral pseudo-velocity at 0.2 s	$PS_\mathrm{v}(T=0.2,\,\xi=0.05)$	cm/s
	$S_{\mathrm{v}\text{-}1.0}$	spectral pseudo-velocity at 1.0 s	$PS_\mathrm{v}(T=1.0,\,\xi=0.05)$	cm/s
	$S_{\mathrm{v}\text{-}2.0}$	spectral pseudo-velocity at 2.0 s	$PS_\mathrm{v}(T=2.0,\,\xi=0.05)$	cm/s
	$S_{\mathrm{d}\text{-}0.2}$	spectral displacement at 0.2 s	$S_\mathrm{d}(T=0.2,\,\xi=0.05)$	cm
	$S_{\mathrm{d}\text{-}1.0}$	spectral displacement at 1.0 s	$S_\mathrm{d}(T=1.0,\,\xi=0.05)$	cm
	$S_{\mathrm{d}\text{-}2.0}$	spectral displacement at 2.0 s	$S_\mathrm{d}(T=2.0,\,\xi=0.05)$	cm
Duration-based IMs	*CAV*	cumulative absolute velocity	$\int_0^{t_\mathrm{tot}}\|a(t)\|\mathrm{d}t$	cm/s
	CAV_5	cumulative absolute velocity with acceleration threshold of 5 cm/s^2	$\int_0^{t_\mathrm{tot}}\|a(t)\|\mathrm{d}t, \|a(t)\|\geqslant 5\ \mathrm{cm/s^2}$	cm/s
	CAD	cumulative absolute displacement	$\int_0^{t_\mathrm{tot}}\|v(t)\|\mathrm{d}t$	cm
	I_a	arias intensity	$\frac{\pi}{2\mathrm{g}}\int_0^{t_\mathrm{tot}}[a(t)]^2\mathrm{d}t$	m/s
	SD_{5-75}	significant duration	time interval between 5% and 75% of I_a, $SD_{5-75}=t_{SD75}-t_{SD5}$	s
	SD_{5-95}	significant duration	time interval between 5% and 95% of I_a, $SD_{5-95}=t_{SD95}-t_{SD5}$	s
	I_c	characteristic intensity	$ARMS^{1.5}\cdot SD_{5-95}^{0.5}$	$\mathrm{g^{1.5}\cdot s^{0.5}}$
	SIR	shaking intensity rate	$0.7I_\mathrm{a}/SD_{5-75}$	m/s^2
	SED	specific energy density	$\int_0^{t_\mathrm{tot}}[v(t)]^2\mathrm{d}t$	cm^2/s
	FI	Fajfar intensity	$PGV\cdot SD_{5-95}^{0.25}$	$\mathrm{cm/s^{0.75}}$

Note: Symbols in Table 2 are explained as follows: $a(t)$: acceleration time history; $v(t)$: velocity time history; $d(t)$: displacement time history; t_tot: total duration of the ground motion record; ξ: damping ratio; S_a: spectral acceleration; S_v: spectral velocity; S_d: spectral displacement; PS_v: spectral pseudo-velocity.

deck weight is modeled as a uniformly distributed load acting along the continuous beam structure of the bridge. Its magnitude is estimated based on the predefined axial load ratio of the pier columns, the concrete compressive

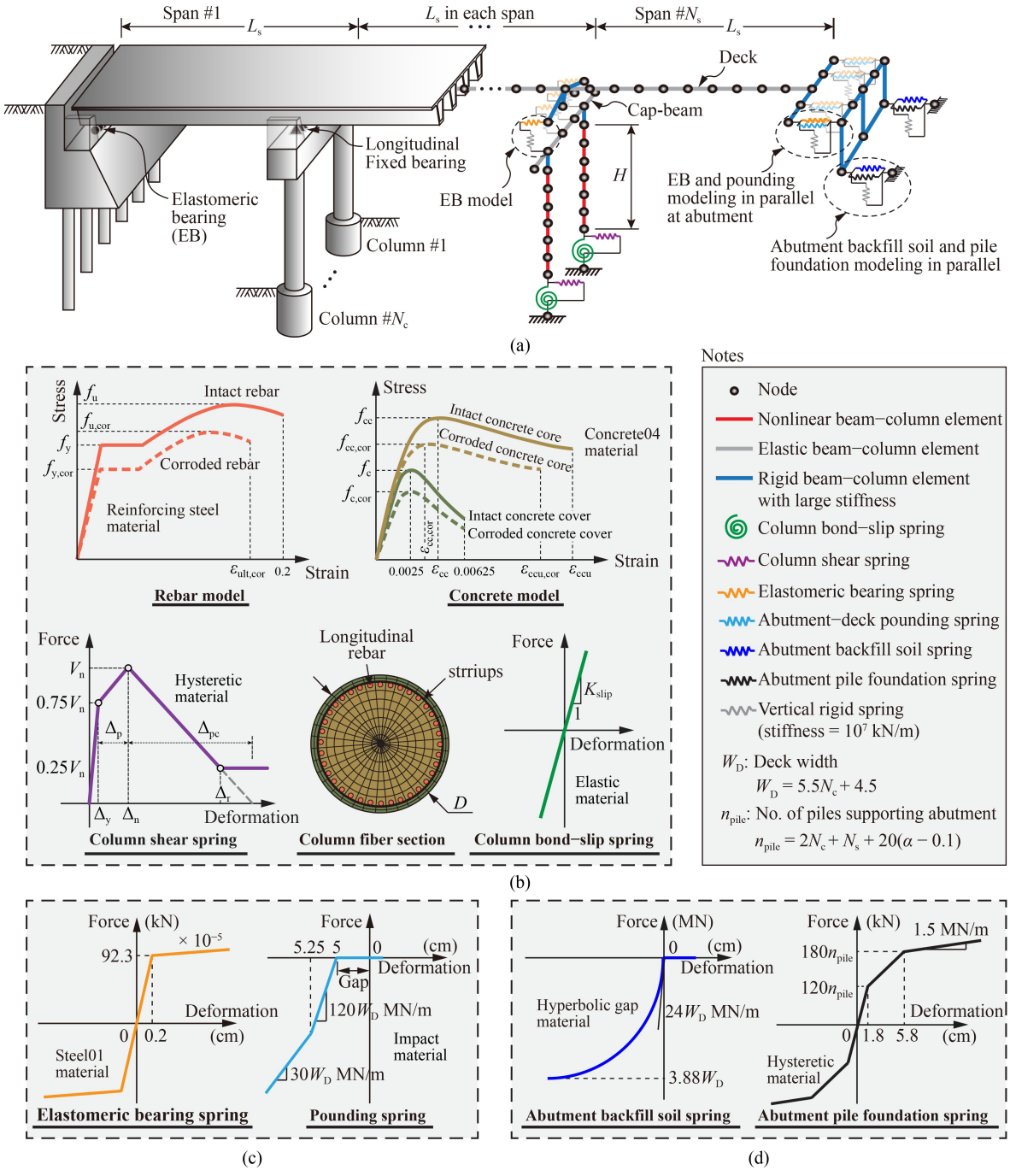

Fig. 2 Parameterized FE modeling of corroded RC bridges: (a) schematic overview; (b) column fiber section illustration, materials constitutive models for corroded rebar and concrete, and column shear behavior and bond–slip effect simulation springs constitutive models; (c) EB and deck–abutment pounding spring constitutive models; and (d) abutment constitutive models.

strength, the cross-sectional area of columns, and the structural layout of the bridge. In the transverse direction, the deck weight is assumed to be evenly distributed among the columns in each bent. The deck width (W_D) is empirically approximated based on the number of columns per bent (N_c) as $W_D = 5.5N_c + 4.5$ (in meters). In this formulation, each column is assumed to occupy approximately 5.5 m of transverse width, which accounts for typical lane width, girder spacing, and construction clearance. The additional 4.5 m provides allowance for deck overhangs, shoulders, and side barriers beyond the outermost columns. The bearing system is strategically arranged to simulate realistic seismic responses. In the longitudinal direction, fixed bearings are placed at the central pier to effectively restrain the longitudinal displacement of the bridge deck. Elastomeric bearings (EB), modeled with bilinear constitutive laws [46] to accurately capture their nonlinear behavior, are employed

at all other intermediate piers and abutments, allowing free longitudinal movements to accommodate seismic-induced deformations. In the transverse direction, each column bent pier includes a single laterally fixed bearing atop a centrally located column. This arrangement provides adequate lateral restraint against transverse seismic forces and prevents excessive lateral displacement. The remaining columns within each bent are equipped with laterally EB to avoid over-constraint and eliminate unintended internal forces during seismic events. This study focuses primarily on seismic responses in the longitudinal direction due to its increased vulnerability compared to the transverse direction for the studied type of highway bridges with one fixed bent (i.e., non-isolated bridges) [47,48]. More specifically, in non-isolated bridges, the longitudinal direction typically presents greater vulnerability because dynamic inertial loading from the superstructure is resisted mainly by a single bent of fixed bearings. Conversely, transverse loading is distributed among multiple bents, resulting in higher overall resistance. Therefore, emphasizing longitudinal responses provides a conservative assessment, particularly effective and efficient in network-level analyses where accurate predictions of seismic input directions for individual bridges are extremely challenging.

The models focus on bridge columns as the primary component governing seismic performance. The bridge column is modeled using the fiber-based nonlinearBeam Column element, which allows simulation of distributed plasticity of materials across the cross-section. The column cross-section is discretized into fibers to capture nonlinear behavior of materials under seismic loading. Longitudinal reinforcement fibers are modeled with the ReinforcingSteel material [49–51]. Concrete cover and core fibers are represented by the Concrete04 uniaxial material, incorporating the confining effects of transverse reinforcement using the Mander model [52]. To account for bond−slip behavior between longitudinal reinforcement and surrounding concrete, a zero-length rotational slip spring element is introduced [53]. This element is calibrated to reflect bond strength deterioration caused by reinforcement corrosion, with its stiffness parameters adjusted accordingly [54]. Additionally, a zero-length horizontal spring element is placed at the column base to simulate potential shear failure under seismic excitation [55,56]. The shear spring parameters explicitly incorporated the effects of reinforcement corrosion, allowing the model to simulate changes in shear capacity and the potential shift in failure modes from flexural to shear-associated failures. Note that extended pile-shafts with larger diameters in the underground portion are adopted as the foundation type for the bridge piers, given their common use in US highway bridge construction. Due to the capacity-protection design principle as well as for modeling expediency, the base of the bridge column is idealized as fully fixed, as shafts embedded into competent soil or rock typically provide sufficient stiffness to approximate fixed-end conditions in both rotation and translation degrees of freedom.

Uniform corrosion of steel reinforcement is explicitly modeled to reflect the reduction in steel cross-sectional area, degradation of yield and ultimate strength, and decreases in the compressive strength of concrete affected by corroded reinforcement. The model also incorporated the effects of corrosion on both longitudinal and transverse reinforcement, capturing the loss of confinement and its impact on the overall column capacity. These corrosion effects are integrated into the bond−slip and shear spring models to ensure the column model could accurately reflect the changes in failure mechanisms. The detailed modeling approach and its implications are documented in Refs. [31,57].

The abutments are modeled with zero-length elements that incorporate coupled constitutive models based on Ref. [58] to simulate both passive and active soil-abutment interactions. Abutment pile foundation is modeled using the Hysteretic uniaxial material to capture nonlinear soil-structure behavior. The number of piles supporting the abutment (n_{pile}) is estimated using a rational approximation $n_{pile} = 2N_c + N_s + 20(\alpha - 0.1)$, which accounts for key factors including the number of bent columns, span-related inertial demands, and the axial load ratio of the columns. Any non-integer result is rounded up to the nearest whole number to ensure conservative design. This expression is developed with reference to bridge foundation design practices in Washington State, US, and has been found to align well with practical design trends observed in medium- to large-scale highway bridge projects. Additionally, a deck-abutment pounding spring, based on Ref. [59], is implemented in parallel with an EB. These elements ensure an accurate representation of the nonlinear interactions between the bridge deck and abutments during seismic loading.

To validate the FE modeling approach, a benchmark shake table test of an RC bridge column [60] was selected for comparison. The numerical model was developed to replicate the experimental setup, and material and reinforcement details were adopted as reported in Ref. [60]. As shown in Fig. 3, the simulation results align well the experimental measurements in terms of inertial force time history (Fig. 3(a)), drift ratio history (Fig. 3(b)), and the hysteretic response (Fig. 3(c)). The model effectively reproduces both the amplitude and phase of the dynamic response, which demonstrates its capability to capture the nonlinear behavior and energy dissipation mechanisms of RC bridge columns subjected to seismic excitation. It is worth noting that, due to the lack of available shake table test data for corroded bridge columns, an uncorroded

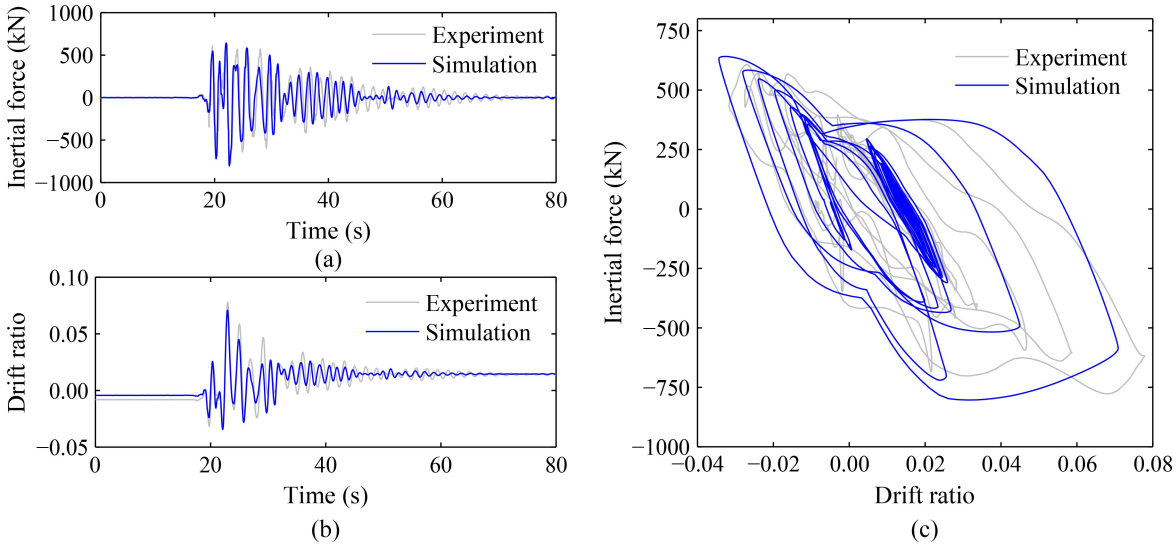

Fig. 3 Validation of numerical modeling by comparison with a full-scale shake-table test of bridge column [60]: (a) inertial force time history; (b) drift ratio time history; (c) hysteretic curves of inertial force versus drift ratio.

benchmark case was used in this validation. This validation primarily aims to examine the capability of the OpenSeesPy model to simulate the dynamic response of RC bridge columns under seismic excitation, rather than to validate the corrosion modeling of material or structural behavior. The corroded column modeling framework adopted in this study has been rigorously validated in the authors' previous work [31] through comparison with experimental data from cyclic loading tests on both corroded and uncorroded RC columns [10,61–63], which covers varying corrosion levels and failure modes, including flexural and shear-associated failures.

3.3 Development of database for damage states

To construct a representative data set for corroded RC bridges under seismic loading, bridge samples are generated by sampling key variables including geometric characteristics, material properties, and corrosion levels, as summarized in Table 1. Latin Hypercube Sampling is employed to ensure a statistically diverse representation of these parameters, resulting in approximately 1800 corroded bridge configurations. These configurations are then evaluated using the ML-based failure mode identification model for corroded RC columns proposed by Ref. [31]. This model effectively distinguishes failure modes and reveals that the majority of bridge column samples exhibit flexural failure, which is the dominant failure mode for corroded RC columns under seismic loading. To refine the database and focus on the most relevant structural behavior, only the flexural failure samples are retained for further analysis. To quantify the seismic capacity of the considered flexural failure bridge columns, the ML-aided rapid estimation model developed by the authors [31] is utilized. This model efficiently estimates the drift ratio capacity at multiple damage levels defined based on the strain-based damage limit states of concrete and steel materials, as listed in Table 3. Notably, a key modification in defining the moderate damage state (LS_2) is made to account for the potential early exfoliation of the concrete cover due to severe corrosion. Instead of using traditional limit states that define moderate damage based on cover concrete crushing, this study considers the strain level in the concrete core, which has been validated as a more representative indicator of damage, particularly for corroded bridge columns whose seismic performance is significantly compromised due to long-term deterioration induced by corrosion [57]. The column drift ratio capacity, representing the deformation capacity corresponding to various damage states, is used as a critical parameter for systematically classifying damage states of corroded bridges. This ensures the database accurately captures the reduced capacity of corroded columns due to material degradation, offering a reliable foundation for

Table 3 Drift ratio capacity limit state description for corroded RC bridge columns

Limit state	Damage state	Description
LS_1	slight	rebar yielding initiate
LS_2	moderate	concrete core strain reaches one-third of ultimate strain
LS_3	extensive	concrete core strain reaches two-thirds of ultimate strain
LS_4	complete	concrete core crushing occur (ultimate strain reached)

subsequent damage classification.

The seismic input for the database is constructed using a reference set of 160 ground acceleration records, carefully selected to represent a broad spectrum of earthquake scenarios. To expand the variability and size of the data set, each record is scaled in amplitude by factors ranging from 1.1 to 2.0, in increments of 0.1, yielding a total of 1760 ground motion records. This augmentation strategy ensures the database encompasses a wide range of seismic intensities, from moderate to severe, and provides a robust basis for evaluating bridge performance under diverse earthquake conditions. By capturing a realistic representation of potential seismic events, the expanded ground motion data set enhances the applicability of the database to practical fragility assessments.

Each of the selected flexural failure bridge samples is paired with a unique ground motion record, and NTHA is performed to simulate their seismic response. The maximum drift ratio of each bridge column, derived from the NTHA results, is used as the primary damage indicator. This drift ratio is compared against ML-predicted multilevel drift ratio capacity thresholds to classify each bridge-ground motion pair into one of five damage states: none, slight, moderate, extensive, or complete. An initial analysis reveals an imbalance in the data set, with a disproportionate number of samples concentrated in certain damage states, particularly the "none" category. To address this, an undersampling technique is applied to reduce the overrepresentation of dominant categories. The finalized database comprises 761 samples that are distributed across all damage states as evenly as possible.

4 Machine learning modeling of damage states

4.1 Overview of adopted machine learning algorithms

In this study, three ML algorithms are employed for damage classification and seismic fragility analysis of corroded RC bridges, including ANN, SVM, and KNN. These algorithms are selected because they represent complementary strengths in handling nonlinear classification problems. ANN is well-suited for capturing complex, high-dimensional relationships among structural parameters, corrosion indicators, and seismic IM, making it particularly effective for learning intricate patterns in large data sets. SVM is widely recognized for its robustness in high-dimensional feature spaces and its ability to achieve accurate classification with limited data, which is valuable for fragility assessment where training data sets may not always be extensive. KNN, by contrast, provides a simple yet powerful non-parametric approach that classifies damage states based on similarity measures, offering interpretability and serving as a useful benchmark against more sophisticated models. Collectively, these algorithms enable a comparative evaluation across different modeling philosophies, i.e., connectionist learning (ANN), margin-based classification (SVM), and instance-based learning (KNN), to identify the most suitable approach for accurately predicting damage states and deriving fragility estimates for corroded RC bridges.

4.1.1 Artificial neural network classifier

The ANN is employed in this study as a primary ML algorithm for classifying damage states of corroded RC bridges under seismic loading. ANNs are particularly well-suited for this task due to their ability to model complex, nonlinear relationships between input features and corresponding damage states. The architecture of the ANN adopted in this study is a feedforward neural network, consisting of an input layer, multiple hidden layers, and an output layer, as illustrated in Fig. 4. Each layer is composed of interconnected nodes (neurons) that process and transmit information through weighted connections.

The input layer contains neurons representing the features from the damage state database, including bridge

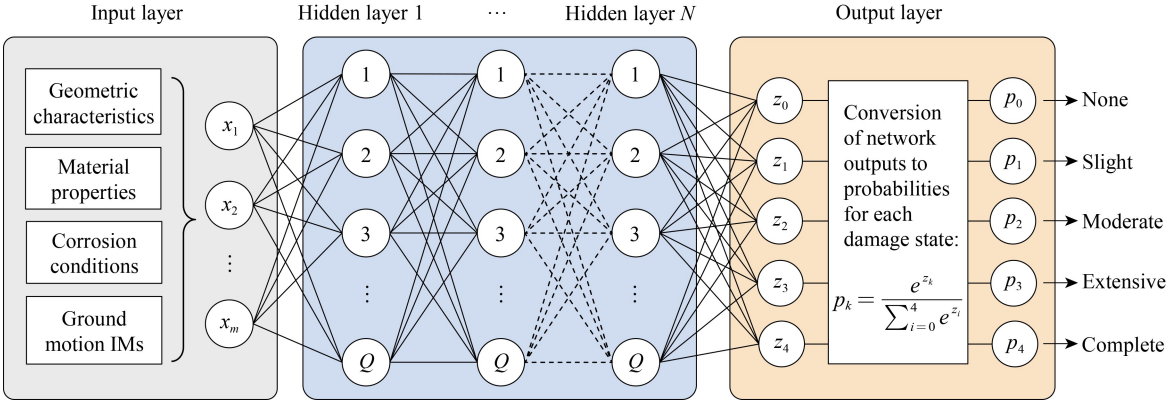

Fig. 4 Architecture of the ANN classifier for seismic damage classification of corroded RC bridges.

geometric characteristics, material properties, corrosion levels, and seismic IM. These input features are standardized to ensure consistency in scale and improve the stability and efficiency of the learning process. The hidden layers are designed with sufficient neurons to capture the complexity of relationships between the input features and damage states. The exact number of hidden layers and neurons per layer is determined through hyperparameter optimization.

In the forward pass, the input features are fed into the input layer and propagated through the network layer by layer. Each hidden layer processes information by performing a weighted sum of the inputs followed by a nonlinear transformation. For a neuron j in a given layer, the weighted sum operation is mathematically expressed as

$$z_j = \sum_i w_{ij} x_i + b_j, \tag{2}$$

where w_{ij} is the weight connecting neuron i in the previous layer to neuron j, x_i is the input from the previous layer, and b_j is the bias term. The resulting sum z_j is then passed through an activation function to capture nonlinear relationships. Each neuron in hidden layers employs the hyperbolic tangent sigmoid transfer function as the activation function, which is defined as

$$\tanh(z_j) = \frac{e^{z_j} - e^{-z_j}}{e^{z_j} + e^{-z_j}}. \tag{3}$$

This activation function is chosen for its smooth nonlinearity and its ability to scale outputs to the range of [−1,1], which facilitates effective learning and convergence during training.

The output layer contains five neurons, each corresponding to one of the damage state categories: none, slight, moderate, extensive, and complete. The SoftMax activation function is applied to the raw outputs (logits) of these neurons to convert them into probabilities, as follows:

$$p_k = \frac{e^{z_k}}{\sum_{k=0}^{4} e^{z_k}}, \tag{4}$$

where p_k represents the probability of the sample belonging to damage state k (0,1,2,3,4), and z_k represents the raw outputs of the neural network. This conversion ensures that the ANN outputs are interpretable probabilities, directly applicable for seismic fragility analysis.

To train the ANN, the target damage states in the database are transformed into a machine-readable format using one-hot encoding. In this encoding scheme, each damage state is represented as a binary vector where a value of 1 indicates the presence of a specific category, and 0 indicates its absence, as shown in Table 4. This transformation ensures compatibility with the categorical cross-entropy loss function, which is used to measure the difference between the predicted probabilities p_k and the one-hot encoded true labels y_k:

Table 4 One-hot encoded damage state

Damage state	One-hot code
None	[1,0,0,0,0]
Slight	[0,1,0,0,0]
Moderate	[0,0,1,0,0]
Extensive	[0,0,0,1,0]
Complete	[0,0,0,0,1]

$$Loss = \frac{1}{bridge\_count} \sum_{\text{all bridges}} \sum_{k=0}^{4} -y_k \log(p_k). \tag{5}$$

The cross-entropy loss function penalizes incorrect predictions while encouraging the network to assign high probabilities to the correct damage states.

During the backward pass, the backpropagation algorithm is used to compute gradients of the loss function with respect to the network parameter (weights and biases). These gradients are then used to iteratively adjust the parameters and minimize the loss function. The parameter update rule is expressed as

$$w_{ij} \leftarrow w_{ij} - \eta \frac{\partial Loss}{\partial w_{ij}}, \tag{6}$$

where η is the learning rate which controls the step size of each update. The optimization is performed using the Adam optimizer, which combines the advantages of adaptive learning rates and momentum to accelerate convergence and enhance stability.

4.1.2 Support vector machine classifier

The SVM is a supervised learning algorithm that is particularly effective for tasks involving complex and nonlinear decision boundaries. This makes it suitable for classifying damage state in corroded RC bridges where relationships between input features and damage states are inherently nonlinear. SVM works by identifying the optimal hyperplane that maximally separates different classes of data in the feature space. Since SVM is inherently designed for binary classification, a one-versus-one (OvO) strategy is adopted in this study to address the multi-class classification problem involving five damage state categories. Figure 5 illustrates the structure of the SVM using OvO for seismic damage classification. Under OvO strategy, separate binary SVM classifiers are constructed for every pair of damage state categories, resulting in 10 binary SVM classifiers for the

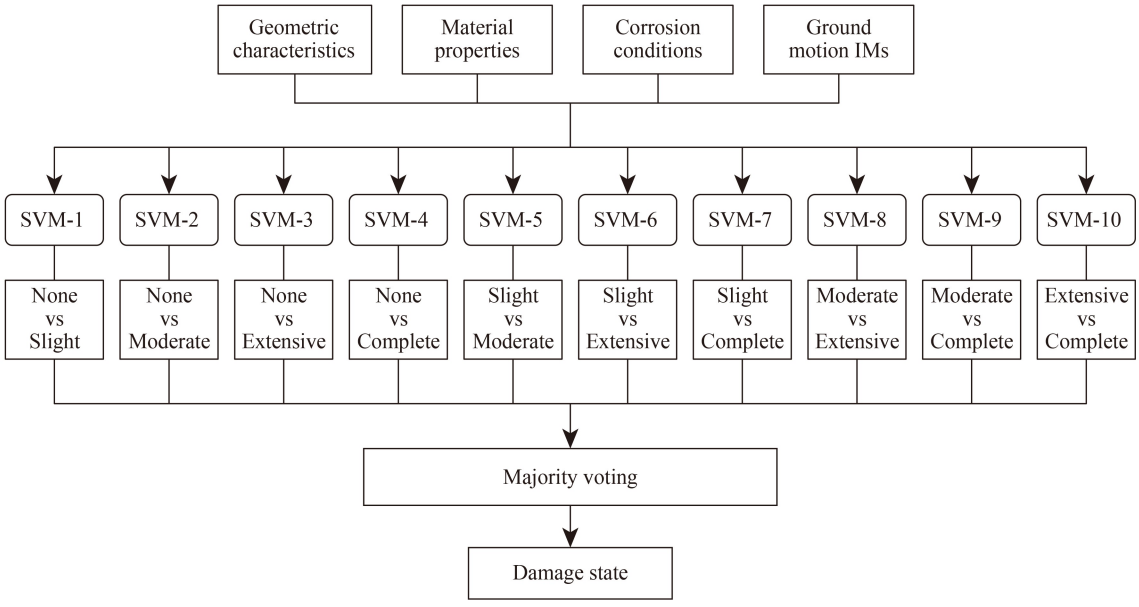

Fig. 5 Structure of the SVM classifier using the OvO strategy for the seismic damage classfication of corroded RC bridges.

five damage states. Each SVM classifier is trained to distinguish between two specific damage states. During the prediction phase, all 10 SVM classifiers are evaluated for a given input, and the final classification decision is made through a voting mechanism, that is, the damage state receiving the highest number of votes across all SVM classifiers is selected as the predicted class.

To capture the complex and nonlinear relationships between input features and damage states, the radial basis function (RBF) kernel, also known as the Gaussian kernel, is employed for the SVM in this study. Kernels play a fundamental role in SVM by transforming data into a higher-dimensional space, enabling the separation of classes that are not linearly separable in the original feature space. The RBF kernel efficiently maps input features into this higher-dimensional space by measuring the similarity between data points based on their Euclidean distance. Mathematically, the RBF kernel between two data points $\boldsymbol{x}_i$ and $\boldsymbol{x}_j$ is defined as

$$K(\boldsymbol{x}_i, \boldsymbol{x}_j) = \exp\left(-\gamma \left\| \boldsymbol{x}_i - \boldsymbol{x}_j \right\|^2\right), \tag{7}$$

where $\left\| \boldsymbol{x}_i - \boldsymbol{x}_j \right\|^2$ represents the squared Euclidean distance between the two feature vectors, and γ is a kernel parameter that controls the influence of individual training samples on the decision boundary. A smaller γ value leads to a smoother decision boundary, while a larger γ value allows for more complex boundaries capable of capturing fine-grained patterns in the data. The selection of γ is critical to the performance of the SVM and is optimized during model training through a grid search procedure.

To enhance the interpretability of the SVM classifier and make it directly applicable for seismic fragility analysis, the outputs of the SVM classifiers are transformed into calibrated probabilities using the Platt scaling technique [64]. Platt scaling fits a sigmoid function to the decision values (raw scores) generated by each SVM classifier and converts them into probabilities. This process involves training a logistic regression model on a calibration data set which is a reserved subset of the training data. The logistic regression model maps the raw decision value $f(\boldsymbol{x})$ to the calibrated probability of the positive class $P(y = 1 | \boldsymbol{x})$ as follows:

$$P(y = 1 | \boldsymbol{x}) = \frac{1}{1 + \exp(Af(\boldsymbol{x}) + B)}, \tag{8}$$

where $f(\boldsymbol{x})$ is the output of the SVM classifier for input $\boldsymbol{x}$, A and B are scaling parameters estimated during training using the maximum likelihood method.

In the multi-class OvO scenario, the calibrated probabilities from all 10 SVM classifiers are combined through pairwise coupling. The final probability for each damage state is derived by solving a constrained optimization problem that ensures the probabilities across all classes sum to 100%. This approach enhances the interpretability of the SVM classifier and allows direct application of the results to seismic fragility analysis.

4.1.3 *K*-nearest neighbor classifier

The KNN algorithm is a non-parametric supervised learning method employed in this study for damage classification of corroded RC bridges. Its simplicity and intuitive nature make it an effective baseline algorithm for multi-class classification tasks. As illustrated in Fig. 6, the KNN classifies samples based on the majority class among their KNN in the feature space. Using features such as bridge geometric characteristics, material

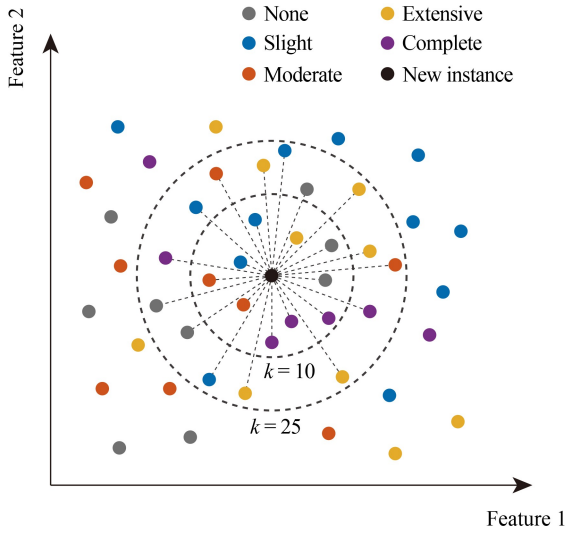

Fig. 6 Schematic diagram of KNN classifier for seismic damage classification of corroded RC bridges.

properties, corrosion levels, and seismic IM, KNN evaluates the similarity between an input sample and the training data set. For a given input, distances to all points in the training data set are calculated based on a pre-defined distance metric, such as Euclidean or Manhattan distance. The K closest neighbors are then identified, and the most frequent damage state among these neighbors is assigned as the predicted class for the input sample. This straightforward process makes KNN highly interpretable and allows KNN to adapt flexibly to various data distributions without assuming any underlying model. To extend its utility for seismic fragility analysis, the KNN algorithm in this study is enhanced to provide probabilistic outputs for each damage state. This is achieved by analyzing the proportion of neighbors belonging to each damage state within the K-neighbor set. For example, if 30% of the neighbors belong to the moderate damage state, the classifier assigns a 30% probability to this class.

The performance of the KNN classifier is highly dependent on two key factors: the choice of K, the number of neighbors considered, and the distance metric used for similarity evaluation. A smaller K value increases the algorithm's sensitivity to local variations in the data set, which can improve its ability to capture fine-grained patterns but may also lead to overfitting or susceptibility to noise. Conversely, a larger K value smooths out local variations, reducing the influence of outliers but potentially losing local detail, particularly in densely populated regions of the feature space. In this study, the optimal K value is determined through cross-validation to strike a balance between local sensitivity and global generalization. The choice of distance metric also plays a significant role in the effectiveness of the KNN classifier. Euclidean distance is widely used for its simplicity and effectiveness in capturing overall similarity between feature vectors, while Manhattan distance measuring similarity based on axis-aligned differences may be preferable for data sets where feature scales or contributions vary significantly. To maximize classification accuracy, multiple distance metrics are evaluated during model validation, and the best-performing metric is selected based on cross-validation results.

4.2 Hyperparameter optimization

Grid search combined with 5-fold cross-validation is employed to systematically tune the hyperparameters of the ANN, SVM, and KNN classifiers. The data set (761 samples) is initially split into an 80% training set and a 20% test set. The training set is further divided into five mutually exclusive and approximately equal subsets for cross-validation, using a fixed random seed to ensure reproducibility. For each model and hyperparameter combination, the same data partitions are consistently used across all folds to allow fair and consistent comparison among models. During each fold, one subset is reserved for validation, while the remaining four subsets are used to train the model. This process is repeated five times, with each subset serving as the validation set once. The mean validation error across all 5-folds is used to evaluate the performance of each hyperparameter configuration in the grid search. Since the ANN directly outputs the probabilities for each damage state, the cross-entropy loss is used as the error metric to evaluate the quality of prediction. For the SVM and KNN classifiers, which provide probabilities indirectly, the classification error is adopted to assess model performance.

The ANN architecture is characterized by two key hyperparameters: the number of hidden layers (N) and the number of neurons per hidden layer (Q). Figure 7(a) illustrates the sensitivity of the mean validation error to different ANN architectures. The results indicate that when N or Q is too small, the error is high due to underfitting, as the network lacks sufficient capacity to learn the intricate patterns in the data. Conversely, when N or Q is too large, the error also increases, reflecting overfitting, as the network becomes overly complex and fails to generalize well to unseen data. Figure 7(b) provides a more detailed analysis of the cross-entropy loss as a function of Q with $N = 3$ on training and validation sets. Considering the balance between accuracy and computational efficiency, $N = 3$ hidden layers and $Q = 50$ neurons per layer are selected as the optimal architecture for the ANN.

The performance of SVM classifier can be influenced by two key hyperparameters: the regularization parameter (C) and the kernel parameter (γ). The parameter C controls the trade-off between maximizing the margin

and minimizing classification errors on the training data, and γ determines the influence of individual training samples on the decision boundary in the RBF kernel. Figure 8(a) presents the sensitivity of the mean classification error to different combinations of C and γ values. Figure 8(b) shows the variation in classification error with γ for a fixed $C = 10^{3.25}$ on training and validation sets. It shows that as γ increases, the training error becomes small, but the validation error rises significantly, reflecting overfitting due to excessively complex decision boundaries. Conversely, smaller γ result in smoother decision boundary and more stable and generalized performance across training and validation data sets. Based on these observations, the optimal hyperparameters for the SVM classifier are selected as $C = 10^{3.25}$ and $\gamma = 10^{-4}$, which could ensure a balance between generalization and accuracy.

For the KNN classifier, the two hyperparameters optimized are the number of nearest neighbors (K) and the distance metric. Several commonly used distance metrics, including Chebyshev, Correlation, Cosine, Euclidean, Manhattan, and Minkowski, are evaluated. Figure 9(a) demonstrates the sensitivity of the mean classification error to varying K values and distance metrics. Among these metrics, Manhattan distance achieves the lowest error, reflecting its suitability for this data set. Figure 9(b) further presents the impact of K on classification error for the Manhattan distance metric on training and validation sets. It shows that smaller K values enhance local sensitivity but may lead to overfitting. In contrast, larger K values improve global generalization by smoothing local variations, but potentially losing critical local detail. Based on these observations, the optimal configuration for the KNN classifier is determined to be $K = 25$ with the Manhattan distance metric, which strikes a balance between local

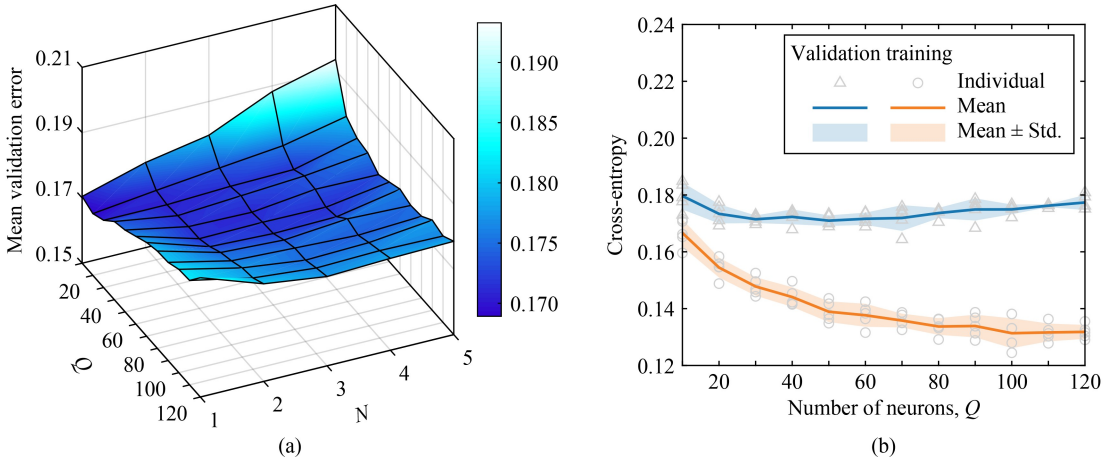

Fig. 7 Hyperparameter optimization of the ANN classifier: (a) 3D plot of the sensitivity of mean validation error to the number of neurons per layer (Q) and the number of hidden layers (N); (b) 2D plot of the variation in cross-entropy loss with Q at $N = 3$ on training and validation sets.

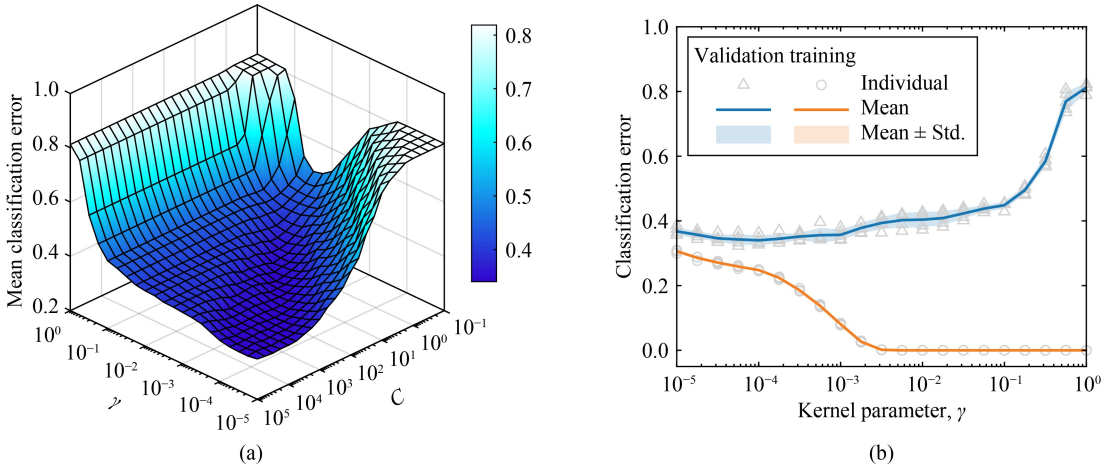

Fig. 8 Hyperparameter optimization of the SVM classifier: (a) 3D plot of the sensitivity of mean classification error to the regularization parameter (C) and kernel parameter (γ); (b) 2D plot of the variation in classification error with γ at $C = 10^{3.25}$ on training and validation sets.

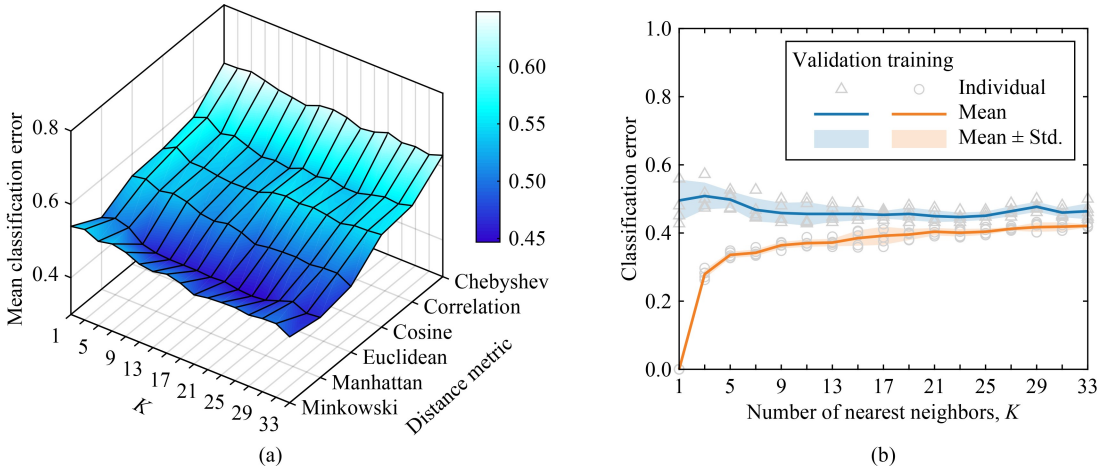

Fig. 9 Hyperparameter optimization of the KNN classifier: (a) 3D plot of the sensitivity of mean classification error to the number of nearest neighbors (K) and different distance metrics; (b) 2D plot of the variation in classification error with K using the Manhattan distance on training and validation sets.

sensitivity and global generalization.

4.3 Performance evaluation of machine learning models in damage state classification

To evaluate the performance of the ML models in classifying damage states of corroded RC bridges under seismic loading, the optimized ANN, SVM, and KNN classifiers are developed, trained on the complete training set, and tested on the reserved test set. The confusion matrix is employed to visualize the classification results and analyze the distribution of correct and incorrect predictions across damage states. The confusion matrices for the ANN, SVM, and KNN classifiers are presented in Figs. 10–12, respectively. These matrices illustrate the classification performance of the ML models on both the training and test sets. Each row corresponds to the true damage state, while each column corresponds to the predicted damage states. Correctly classified samples are positioned along the diagonal (highlighted in blue), while off-diagonal elements indicate misclassifications. From the confusion matrices, it can be observed that the ANN achieves the highest diagonal dominance, indicating strong classification performance across all damage states. The SVM also demonstrates high performance, but with slightly more off-diagonal elements compared to the ANN. In contrast, the KNN shows the most pronounced off-diagonal elements, particularly for the moderate and extensive damage states, indicating challenges in distinguishing these damage states.

Based on the confusion matrices, three key metrics are calculated to quantitatively evaluate model performance: precision, recall, and accuracy. Precision, defined as the ratio of true positives (correct predictions for a specific damage state) to the total predicted positives (including false positives), measures the reliability of the model's

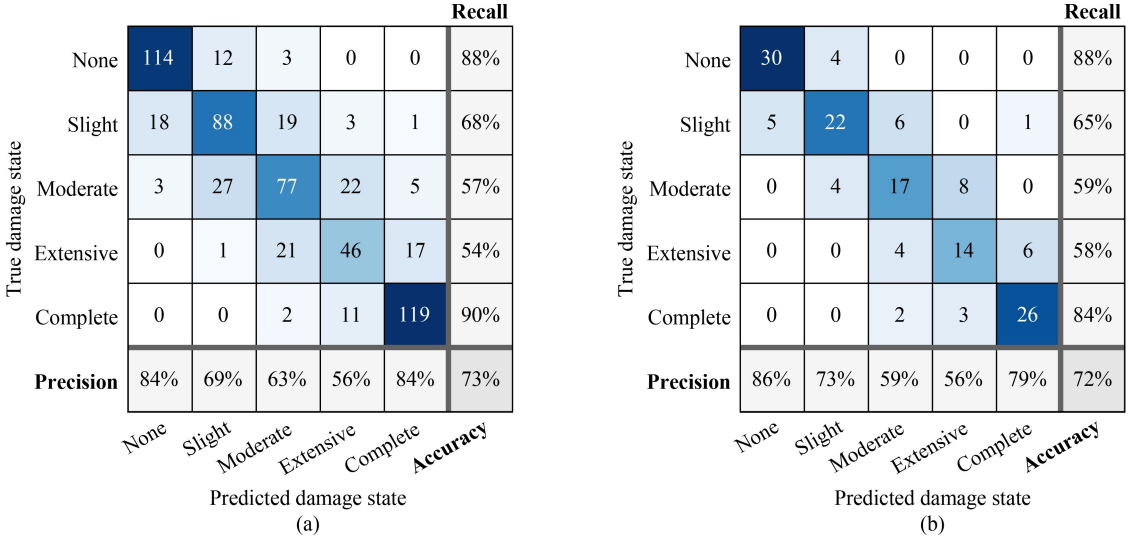

Fig. 10 Confusion matrices with recall, precision, and accuracy metrics of the ANN classifier for seismic damage classification on: (a) the training set; (b) the test set.

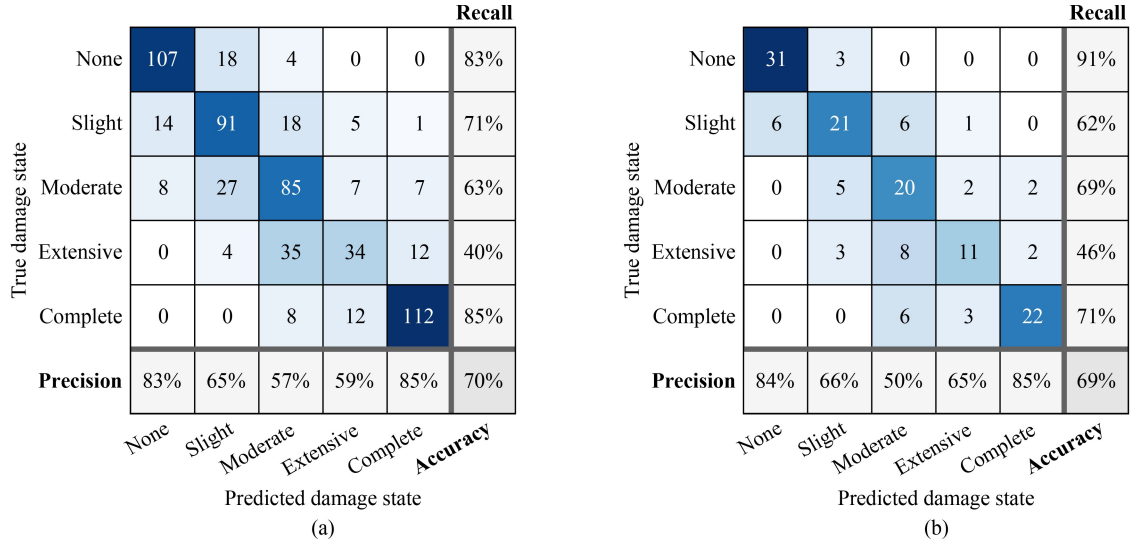

Fig. 11 Confusion matrices with recall, precision, and accuracy metrics of the SVM classifier for seismic damage classification on: (a) the training set; (b) the test set.

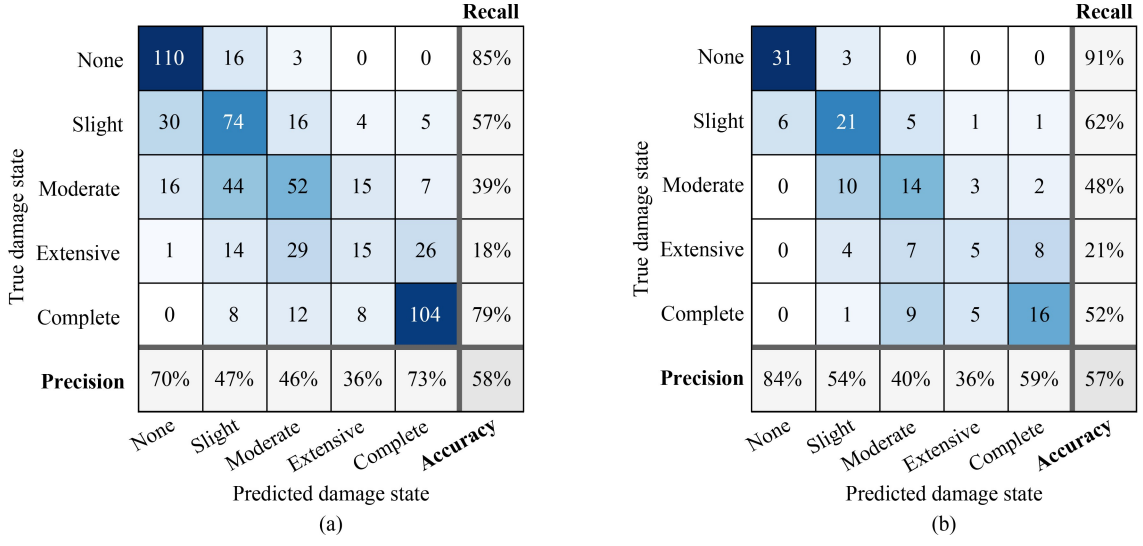

Fig. 12 Confusion matrices with recall, precision, and accuracy metrics of the KNN classifier for seismic damage classification on: (a) the training set; (b) the test set.

predictions for each damage state. Recall, the ratio of true positives to the total actual positives (including false negatives), reflects the model's ability to identify all samples of a specific damage state. Accuracy provides an overall measure of the model's performance, representing the proportion of correctly classified samples across all damage states. Among the three evaluated ML models, the ANN achieves the highest overall accuracy, precision, and recall, underscoring its ability to effectively model complex, nonlinear relationships in high-dimensional data. The SVM demonstrates comparable performance, benefiting from its ability to construct precise decision boundaries in high-dimensional feature spaces. However, the KNN classifier, while providing a simple and interpretable baseline, faces notable challenges in the high-dimensional feature space of the damage state database. The "curse of dimensionality" can dilute the effectiveness of distance metrics, leading to reduced classification accuracy, particularly for damage states with less distinct boundaries such as "moderate" and "extensive". These findings emphasize the superiority of ANN and SVM for seismic fragility assessments, with ANN emerging as the most reliable tool for capturing nonlinear relationships and delivering accurate predictions across diverse bridge configurations and seismic scenarios.

5 Illustration application to fragility analysis

To demonstrate the application of the ML models in

seismic fragility analysis for corroded RC bridges, a typical three-span RC highway bridge is examined as a case study. The seismic fragility of this bridge is analyzed accounting for the effects of corrosion that develops after a period of service time. The structural configuration, material properties, and corrosion levels of the bridge are detailed in Table 5. For reference and comparison purposes, the Cloud method, a widely used traditional seismic fragility analysis approach, is also employed.

Seismic fragility is typically represented by fragility curves, which indicate the probability of seismic demand (*SD*) exceeding seismic capacity (*SC*) at various damage states at a given level of the *IM*. These probabilities incorporate uncertainties in seismic demand and capacity due to structural and seismic variabilities. The Could method assumes that both seismic demand and capacity follow lognormal distributions, with the exceedance probability for a specific damage state given by

$$P[SD > SC|IM] = \Phi\left[\frac{\ln(M_{SD|IM}/M_{SC})}{\sqrt{\beta_{\ln SD}^2+\beta_{\ln SC}^2}}\right], \tag{9}$$

where $\Phi[\cdot]$ represents the standard normal cumulative distribution function, $M_{SD|IM}$ and M_{SC} are the medians of the seismic demand and capacity, respectively. $\beta_{\ln SD}$ and $\beta_{\ln SC}$ are the logarithmic standard deviations of seismic demand and seismic capacity, respectively.

The Cloud method involves estimating both seismic demand and capacity. The seismic capacity of the case-study bridge is estimated using the ML-aided rapid estimation model proposed by Ref. [31]. This model predicts multi-level drift ratio capacity thresholds for various damage limit states, as listed in Table 6 for the case-study bridge. Note that uncertainties in capacity thresholds of damage states (i.e., $\beta_{\ln SC}$ in Eq. (9)) is not considered for the expediency of application illustration.

To quantify the uncertainty in seismic demand, probabilistic seismic demand analysis is performed to model the relationship between the seismic demand and the *IM*. The seismic demand median ($M_{SD|IM}$) is assumed to follow a power law relationship with *IM* [11]:

$$M_{SD|IM} = a \cdot IM^b. \tag{10}$$

This relationship is then transformed into a linear logarithmic form:

$$\ln M_{SD|IM} = \ln a + b\ln(IM). \tag{11}$$

Parameters a and b are estimated via linear regression on *SD-IM* data collected from NTHA. Assuming the variance of seismic demand to be constant across different *IM* levels, the logarithmic standard deviation of seismic demand ($\beta_{\ln SD}$) can be calculated from the residuals of the regression, as follows

$$\beta_{\ln SD} = \sqrt{\frac{\sum_{i=1}^{n}[\ln(SD_i) - \ln a - b\ln(IM_i)]^2}{n-2}}, \tag{12}$$

Table 5 Structural configuration details of the case-study corroded RC highway bridge

Category	ID	Parameter	Name	Value
Structure-related (uncorroded)	x_1	N_s	number of spans	3
	x_2	L_s (m)	span length	30
	x_3	N_c	number of columns per bent	3
	x_4	D (m)	column diameter	1.5
	x_5	H (m)	column height	7
	x_6	f_c (MPa)	concrete compressive strength	32
	x_7	f_y (MPa)	reinforcing steel yield strength	465
	x_8	ρ_l	column longitudinal reinforcement ratio	2%
	x_9	ρ_t	column transverse reinforcement ratio	0.85%
	x_{10}	α	axial load ratio	17.5%
Corrosion-related	x_{11}	X_l	corrosion level of longitudinal reinforcement	15%
	x_{12}	X_t	corrosion level of transverse reinforcement	30%

Table 6 Column drift ratio limit states of the case-study corroded RC highway bridge

Limit state	Damage state	Description	Drift ratio threshold
LS_1	slight	rebar yielding initiates	0.88%
LS_2	moderate	concrete core strain reaches one-third of ultimate strain	1.52%
LS_3	extensive	concrete core strain reaches two-thirds of ultimate strain	2.01%
LS_4	complete	concrete core crushing occurs (ultimate strain reached)	2.52%

where n is the number of NTHA simulations, and SD_i and IM_i are the seismic demand and IM for the ith ground motion, respectively. To maintain consistency with seismic capacity, the column drift ratio response is chosen as the seismic demand, with the maximum drift ratio used as the bridge damage indicator. Consequently, the exceedance probability of damage states as a function of IM based on the seismic capacity threshold (LS_k) corresponding to the kth damage state is expressed as

$$P[SD > \mathrm{LS}_k | IM = x] = \Phi\left[\frac{\ln(a) + b\ln(x) - \ln(\mathrm{LS}_k)}{\beta_{\ln SD}}\right]. \tag{13}$$

Following the Cloud method framework, 100 ground motion records randomly selected from the constructed seismic database are applied to perform NTHA for the specific case-study bridge. Seismic fragility curves for various damage states are then derived, with peak ground velocity (PGV) chosen as the IM. PGV is selected due to its identified effectiveness as one of the optimal IMs for PSDM of corroded RC columns [57].

The ML-empowered seismic fragility analysis represents a fundamentally different method bypassing the traditional demand-capacity comparison framework. Instead of relying on the iterative simulation process required by conventional framework, the developed ML models, specifically the developed ANN, SVM, and KNN classifiers, directly predict the probabilities of each damage state based on bridge structural and seismic inputs. In this case study, the same set of 100 ground motion records utilized in the Cloud method is applied to obtain IMs as seismic input for ML models for consistency. These IMs, combined with the structural parameters of the case-study bridge, serve as the input features for ML models. The ML models output classification probabilities for each damage state, which are subsequently aggregated to obtain exceedance probabilities for each damage state and construct fragility curves.

Figures 13–15 illustrate the fragility curves derived from ANN, SVM, and KNN models, respectively, in comparison to those obtained using the Cloud method. In these figures, scatter points represent exceedance probabilities aggregated from ML-predicted probabilities for each damage state at varying PGV levels. These scatter points are fitted using a cumulative normal distribution function to generate fragility curves [65], where genetic algorithm is employed to ensure globally optimal curve fitting. It is observed that fragility curves derived from the ANN closely align with those obtained from the Cloud method, particularly for slight, moderate, and extensive damage states. The SVM also demonstrates strong agreement but exhibits slightly larger deviations for moderate and complete damage states, suggesting reduced sensitivity in higher seismic intensity levels. By

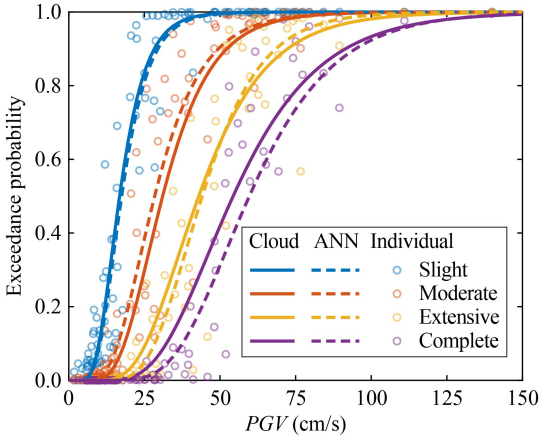

Fig. 13 Comparison of fragility curves derived from the ANN classifier and the Cloud method: the exceedance probability of different damage states (slight, moderate, extensive, and complete) as a function of PGV.

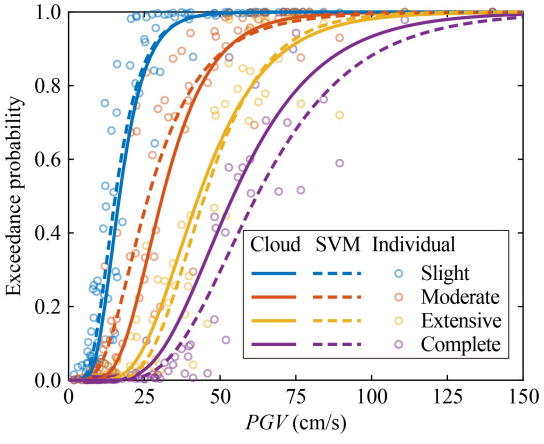

Fig. 14 Comparison of fragility curves derived from the SVM classifier and the Cloud method: The exceedance probability of different damage states (slight, moderate, extensive, and complete) as a function of PGV.

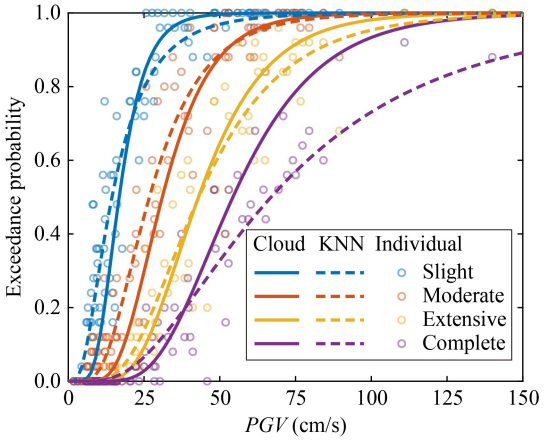

Fig. 15 Comparison of fragility curves derived from the KNN classifier and the Cloud method: The exceedance probability of different damage states (slight, moderate, extensive, and complete) as a function of PGV.

contrast, the KNN model displays notable deviations, particularly for complete damage state at higher *PGV* levels. This discrepancy is likely due to its reliance on localized patterns within the database and its sensitivity to noise and sparsity in the data.

To further evaluate the performance of the ML-empowered methods in comparison with the Cloud method, the fragility curves derived from both methods are quantitatively compared using the relative root mean square error (*RRMSE*). The *RRMSE* measures the average relative difference between the ML-predicted fragility curves and those obtained from the Cloud method over the range of IM values, which is computed as

$$RRMSE = \frac{\sqrt{\frac{1}{IM_{\max} - IM_{\min}} \int_{IM_{\min}}^{IM_{\max}} [f_{\text{Cloud}}(x) - f_{\text{ML}}(x)]^2 \mathrm{d}x}}{\frac{1}{IM_{\max} - IM_{\min}} \int_{IM_{\min}}^{IM_{\max}} |f_{\text{Cloud}}(x)| \mathrm{d}x}, \tag{14}$$

where $f_{\text{Cloud}}(x)$ and $f_{\text{ML}}(x)$ represent the fragility curves derived from the Cloud method and ML models, respectively. A lower RRMSE value indicates a closer match between the two methods. In this study, *PGV* is selected as the IM for comparison. The integration bounds are set as $PGV_{\min}$ = 0.237 cm/s and $PGV_{\max}$ = 155 cm/s, which reflect a wide and realistic range of ground motion intensities encountered in engineering applications. These values are selected based on the national seismic hazard model provided by the US Geological Survey [66], ensuring consistency with national seismic hazard data. The results listed in Table 7 indicate that the ANN consistently achieves the lowest *RRMSE* across all damage states, demonstrating the closest alignment with the Cloud method. The SVM shows competitive performance for moderate and extensive damage states but exhibits larger deviations for slight and complete damage states. In contrast, the KNN model yields the highest *RRMSE* values, particularly for the complete damage state, reflecting its limitations in capturing complex, high-dimensional, and nonlinear seismic response patterns.

The comparison between the Could and ML-empowered methods demonstrates the effectiveness of ML-empowered methods in seismic fragility analysis for corroded RC bridges. Both ANN and SVM models successfully replicate fragility curves generated by the Cloud method while significantly reducing computational effort. Among the three ML models, ANN stands out for its superior balance between accuracy and computational efficiency, solidifying its position as the most robust and reliable method for seismic fragility assessments. These findings highlight the potential of ML-empowered methods as efficient and accurate alternatives to traditional frameworks. As a scalable solution, ML models can be effectively employed in large-scale regional seismic resilience assessments, particularly for aging and corroded bridge infrastructure.

Table 7 Comparison of *RRMSE* for fragility curves derived from the Cloud method and ML-empowered methods

Damage state	*RRMSE*		
	ANN vs Cloud	SVM vs Cloud	KNN vs Cloud
Slight	1.3%	2.5%	5.5%
Moderate	4.1%	7.1%	6.6%
Extensive	3.2%	3.6%	4.5%
Complete	8.1%	11.5%	23.8%

To further demonstrate the capability of the proposed ML-empowered fragility modeling method in capturing time-dependent deterioration effects, fragility surfaces are developed as shown in Fig. 16. The results reveal that increasing levels of corrosion lead to elevated seismic vulnerability for most damage states. However, this effect is less significant for the slight damage state, suggesting that reinforcement corrosion has limited influence on the onset of slight damage, while its impact becomes significantly more severe for higher damage states.

These results highlight the ability of the proposed ML-empowered method to efficiently generate time-dependent fragility representations without the need to rerun NTHA at each corrosion level. By enabling continuous and scalable fragility evaluation across varying corrosion scenarios, the framework provides a powerful tool for large-scale seismic risk assessment and lifecycle-informed resilience planning for aging transportation infrastructure.

6 Conclusions

This study proposed a novel ML-empowered method for efficient seismic damage classification and fragility estimation of corroded RC bridges, addressing critical challenges in assessing aging infrastructure under seismic hazards. A comprehensive corroded bridge portfolio is developed, which accounts for geometric variations, material property deterioration, and corrosion-induced capacity degradation. Three ML classification algorithms including ANN, SVM, and KNN are explored for their ability to predict the damage states of corroded RC bridges subjected to seismic loading. A comprehensive damage state database is developed through NTHA based on advanced FE simulations, incorporating the effects of corrosion-induced degradation, structural variability, and diverse seismic scenarios. Hyperparameters for each ML model are systematically optimized via grid search with 5-fold cross-validation to enhance classification accuracy and generalization capability. The performance of ML models in classifying the seismic damage states of

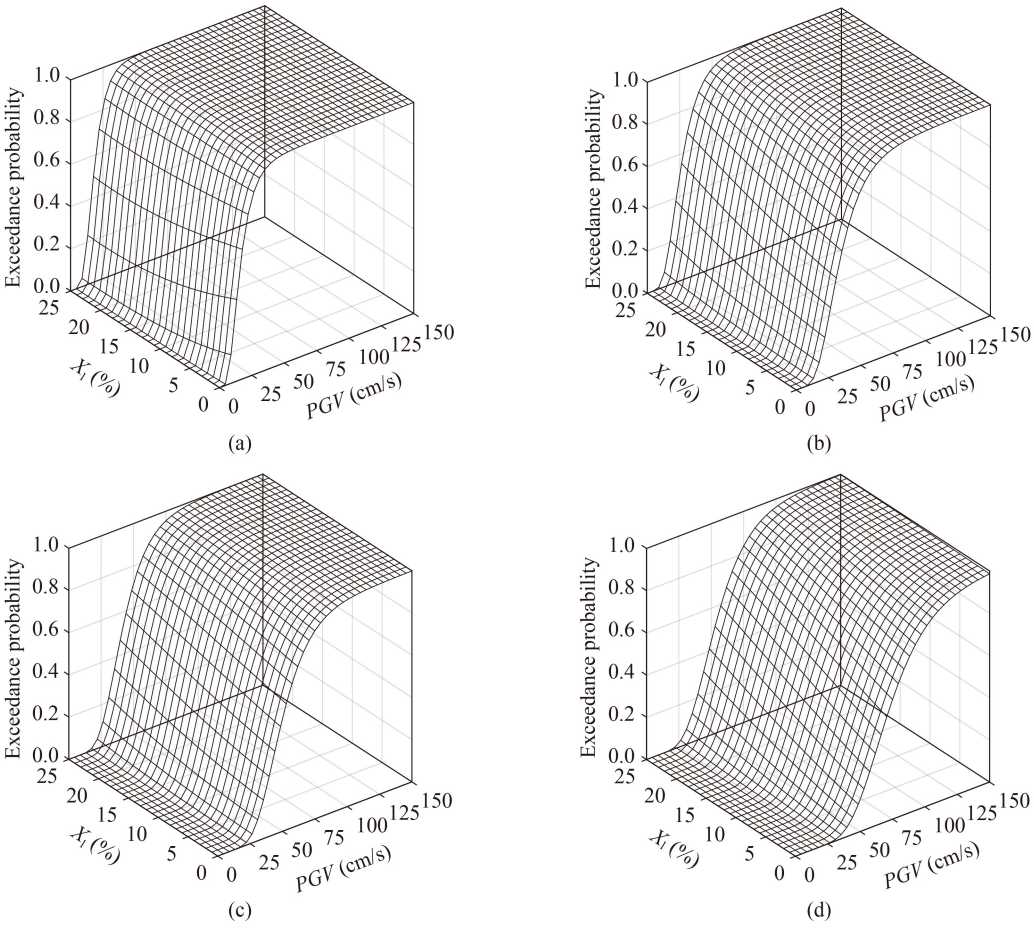

Fig. 16 Fragility surfaces as functions of *PGV* and longitudinal reinforcement corrosion ratio (X_l) for different damage states: (a) slight; (b) moderate; (c) extensive; (d) complete damage states.

corroded RC bridges are evaluated through the confusion matrices and standard evaluation metrics, including recall, precision, and accuracy.

The results show that the ANN outperforms other ML models and demonstrates the best overall performance, achieving the highest accuracy and reliability in damage state classification. Its ability to effectively model complex nonlinear relationships and generalize across diverse conditions made it the most robust choice for seismic fragility analysis. The SVM achieved comparable results in slight and moderate damage states but showed deviations under high-intensity seismic loading. In contrast, the KNN model exhibited lower accuracy, particularly for the complete damage state at high seismic intensity, due to its sensitivity to localized patterns in high-dimensional feature spaces.

A case study of a three-span corroded RC highway bridge is conducted to demonstrate the practical application of the proposed method. Fragility curves generated by the ML models are compared with those obtained from the traditional Cloud method. Both the ANN and SVM models closely replicate the fragility curves derived from the Cloud method, particularly for slight, moderate, and extensive damage states. Among the ML models, the ANN achieves the best balance between accuracy and computational efficiency. In contrast, the KNN model exhibits larger deviations, particularly for the complete damage state at higher levels of seismic intensity. The findings highlight the potential of ML-empowered methods in seismic fragility analysis by eliminating the need for iterative NTHA required in traditional methods, thus significantly reducing computational effort and enabling their application in large-scale regional assessments of aging and corroded infrastructure.

It should be noted that the fragility estimation ML models trained in this study are applicable to typical multi-span continuous RC bridge configurations with key parameters falling within the range of the developed database. The models are established for circular RC columns with reinforcement corrosion and flexural failure modes, and the seismic damage states are defined based on column drift ratio limit states. Nevertheless, the proposed framework can be further extended to other structural types or deterioration mechanisms by incorporating additional data and retraining the ML models.

This study has several limitations. First, the proposed

ML-based framework is developed and validated for corroded RC bridges with circular columns and flexural failure modes. Second, the database used for model training is generated through numerical simulations. Although the simulation parameters were calibrated using experimental data from previous studies, uncertainties associated with real-world bridge conditions and construction variability may not be fully represented. Third, corrosion effects are applied only to bridge columns, while other components such as bearings, abutments, and deck connections are modeled with idealized boundary conditions. Future studies will focus on extending the framework to other bridge types, incorporating additional deterioration mechanisms, and integrating field monitoring data to support system-level seismic risk assessment. Overall, this study contributes a scalable, data-driven solution for fragility analysis, which provides a practical and computationally efficient tool to support the seismic resilience planning of critical transportation infrastructure.

Acknowledgements The research described in this paper was supported, in part, by the National Science Foundation (No. NSF-1638320) and the US Department of Transportation National Center for Transportation Infrastructure Durability and Life Extension. The second author acknowledged the partial support from the National Natural Science Foundation of China (Grant No. 52378183).

Competing interests The authors declare that they have no competing interests.

References

1. Biondini F, Camnasio E, Titi A. Seismic resilience of concrete structures under corrosion. Earthquake Engineering & Structural Dynamics, 2015, 44(14): 2445–2466
2. Cheng H, Li H N, Yang Y B, Wang D S. Seismic fragility analysis of deteriorating RC bridge columns with time-variant capacity index. Bulletin of Earthquake Engineering, 2019, 17(7): 4247–4267
3. Ghosh J, Padgett J E. Aging considerations in the development of time-dependent seismic fragility curves. Journal of Structural Engineering, 2010, 136(12): 1497–1511
4. Molaioni F, Rinaldi Z, Andriotis C P. Assessing Life-Cycle Seismic Fragility of Corroding Reinforced Concrete Bridges Through Dynamic Bayesian Networks. Boca Raton, FL: CRC Press, 2023
5. Zhang Y, Ayyub B M, Fung J F. Projections of corrosion and deterioration of infrastructure in United States coasts under a changing climate. Resilient Cities and Structures, 2022, 1(1): 98–109
6. Capacci L, Biondini F, Frangopol D M. Resilience of aging structures and infrastructure systems with emphasis on seismic resilience of bridges and road networks. Resilient Cities and Structures, 2022, 1(2): 23–41
7. Goksu C, Ilki A. Seismic behavior of reinforced concrete columns with corroded deformed reinforcing bars. ACI Structural Journal, 2016, 113(5): 1053–1064
8. Luo X, Cheng J, Xiang P, Long H. Seismic behavior of corroded reinforced concrete column joints under low-cyclic repeated loading. Archives of Civil and Mechanical Engineering, 2020, 20(2): 40
9. Meda A, Mostosi S, Rinaldi Z, Riva P. Experimental evaluation of the corrosion influence on the cyclic behaviour of RC columns. Engineering Structures, 2014, 76: 112–123
10. Vu N S, Li B. Seismic performance of flexural reinforced concrete columns with corroded reinforcement. ACI Structural Journal, 2018, 115(5): 1253–1266
11. Cornell C A, Jalayer F, Hamburger R O, Foutch D A. Probabilistic basis for 2000 SAC federal emergency management agency steel moment frame guidelines. Journal of Structural Engineering, 2002, 128(4): 526–533
12. Vamvatsikos D, Cornell C A. Incremental dynamic analysis. Earthquake Engineering & Structural Dynamics, 2002, 31(3): 491–514
13. Singhal A, Kiremidjian A S. Method for probabilistic evaluation of seismic structural damage. Journal of Structural Engineering, 1996, 122(12): 1459–1467
14. Altieri D, Patelli E. An efficient approach for computing analytical non-parametric fragility curves. Structural Safety, 2020, 85: 101956
15. Pang Y, Wang X. Cloud-IDA-MSA conversion of fragility curves for efficient and high-fidelity resilience assessment. Journal of Structural Engineering, 2021, 147(5): 04021049
16. Soleimani F, Hajializadeh D. State-of-the-art review on probabilistic seismic demand models of bridges: Machine-learning application. Infrastructures, 2022, 7(5): 64
17. Kim T, Song J, Kwon O S. Probabilistic evaluation of seismic responses using deep learning method. Structural Safety, 2020, 84: 101913
18. Feng D C, Cao X Y, Wang D, Wu G. A PDEM-based non-parametric seismic fragility assessment method for RC structures under non-stationary ground motions. Journal of Building Engineering, 2023, 63: 105465
19. Mai C, Konakli K, Sudret B. Seismic fragility curves for structures using non-parametric representations. Frontiers of Structural and Civil Engineering, 2017, 11(2): 169–186
20. Mangalathu S, Jeon J S. Stripe-based fragility analysis of

multispan concrete bridge classes using machine learning techniques. Earthquake Engineering & Structural Dynamics, 2019, 48(11): 1238–1255
21. Ghosh J. Next generation fragility functions for seismically designed highway bridges in moderate seismic zones. Natural Hazards Review, 2021, 22(1): 04020051
22. Mangalathu S, Jeon J S, DesRoches R. Critical uncertainty parameters influencing seismic performance of bridges using Lasso regression. Earthquake Engineering & Structural Dynamics, 2018, 47(3): 784–801
23. Xie Y, Ebad Sichani M, Padgett J E, DesRoches R. The promise of implementing machine learning in earthquake engineering: A state-of-the-art review. Earthquake Spectra, 2020, 36(4): 1769–1801
24. Bhatta S, Kang X, Dang J. Machine learning prediction models for ground motion parameters and seismic damage assessment of buildings at a regional scale. Resilient Cities and Structures, 2024, 3(1): 84–102
25. Mangalathu S, Hwang S H, Choi E, Jeon J S. Rapid seismic damage evaluation of bridge portfolios using machine learning techniques. Engineering Structures, 2019, 201: 109785
26. Mangalathu S, Heo G, Jeon J S. Artificial neural network based multi-dimensional fragility development of skewed concrete bridge classes. Engineering Structures, 2018, 162: 166–176
27. Yuan X, Chen G, Jiao P, Li L, Han J, Zhang H. A neural network-based multivariate seismic classifier for simultaneous post-earthquake fragility estimation and damage classification. Engineering Structures, 2022, 255: 113918
28. Sainct R, Feau C, Martinez J M, Garnier J. Efficient methodology for seismic fragility curves estimation by active learning on support vector machines. Structural Safety, 2020, 86: 101972
29. Kostinakis K, Morfidis K, Demertzis K, Iliadis L. Classification of buildings' potential for seismic damage using a machine learning model with auto hyperparameter tuning. Engineering Structures, 2023, 290: 116359
30. Xu J G, Feng D C, Mangalathu S, Jeon J S. Data-driven rapid damage evaluation for life-cycle seismic assessment of regional reinforced concrete bridges. Earthquake Engineering & Structural Dynamics, 2022, 51(11): 2730–2751
31. Xu B, Wang X, Yang C S W, Li Y. Machine learning-aided rapid estimation of multilevel capacity of flexure-identified circular concrete bridge columns with corroded reinforcement. Journal of Structural Engineering, 2024, 150(3): 04024002
32. Hsu Y T, Fu C C. Seismic effect on highway bridges in Chi Chi earthquake. Journal of Performance of Constructed Facilities, 2004, 18(1): 47–53
33. Kawashima K, Unjoh S. The damage of highway bridges in the 1995 Hyogo-Ken Nanbu earthquake and its impact on Japanese seismic design. Journal of Earthquake Engineering, 1997, 1(3): 505–541
34. Han Q, Du X, Liu J, Li Z, Li L, Zhao J. Seismic damage of highway bridges during the 2008 Wenchuan earthquake. Earthquake Engineering and Engineering Vibration, 2009, 8(2): 263–273
35. Padgett J E, DesRoches R. Sensitivity of seismic response and fragility to parameter uncertainty. Journal of Structural Engineering, 2007, 133(12): 1710–1718
36. Li H, Li L, Zhou G, Xu L. Effects of various modeling uncertainty parameters on the seismic response and seismic fragility estimates of the aging highway bridges. Bulletin of Earthquake Engineering, 2020, 18(14): 6337–6373
37. Mangalathu S, Jeon J S, Padgett J E, DesRoches R. ANCOVA-based grouping of bridge classes for seismic fragility assessment. Engineering Structures, 2016, 123: 379–394
38. Mangalathu S. Performance based grouping and fragility analysis of box-girder bridges in California. Dissertation for the Doctoral Degree. Atlanta, GA: Georgia Institute of Technology, 2017
39. Lin H, Zhao Y, Yang J Q, Feng P, Ozbolt J, Ye H. Effects of the corrosion of main bar and stirrups on the bond behavior of reinforcing steel bar. Construction and Building Materials, 2019, 225: 13–28
40. Otsuki N, Miyazato S, Diola N B, Suzuki H. Influences of bending crack and water–cement ratio on chloride-induced corrosion of main reinforcing bars and stirrups. Materials Journal, 2000, 97(4): 454–464
41. Yuan X, Zhong J, Zhu Y, Chen G, Dagli C. Post-earthquake regional structural damage evaluation based on artificial neural networks considering variant structural properties. Structures, 2023, 52: 971–982
42. Kostinakis K, Athanatopoulou A, Morfidis K. Correlation between ground motion intensity measures and seismic damage of 3D R/C buildings. Engineering Structures, 2015, 82: 151–167
43. de Biasio M. Ground motion intensity measures for seismic probabilistic risk analysis. Dissertation for the Doctoral Degree. Grenoble: University Grenoble Alpes, 2014
44. Dai J C, Wang D S, Chen X Y, Zhang R, Sun Z G. Evaluation of ground motion intensity measures for time-history dynamic analysis of isolated bridges. Structures, 2023, 55: 1306–1319
45. Zhu M, McKenna F, Scott M H. OpenSeesPy: Python library for the OpenSees finite element framework. SoftwareX, 2018, 7: 6–11
46. Zhang J, Huo Y. Evaluating effectiveness and optimum design of isolation devices for highway bridges using the fragility function method. Engineering Structures, 2009, 31(8): 1648–1660
47. Shamsabadi A, Rollins K M, Kapuskar M. Nonlinear soil–abutment–bridge structure interaction for seismic performance-based design. Journal of Geotechnical and Geoenvironmental Engineering, 2007, 133(6): 707–720
48. Nielson B G, DesRoches R. Seismic fragility methodology for highway bridges using a component level approach. Earthquake Engineering & Structural Dynamics, 2007, 36(6): 823–839
49. Dhakal R P, Maekawa K. Modeling for postyield buckling of reinforcement. Journal of Structural Engineering, 2002, 128(9): 1139–1147
50. Dodd L L, Restrepo-Posada J I. Model for predicting cyclic behavior of reinforcing steel. Journal of Structural Engineering, 1995, 121(3): 433–445
51. Gomes A, Appleton J. Nonlinear cyclic stress-strain relationship of reinforcing bars including buckling. Engineering Structures, 1997, 19(10): 822–826
52. Mander J B, Priestley M J N, Park R. Theoretical stress−strain model for confined concrete. Journal of Structural Engineering, 1988, 114(8): 1804–1826
53. Elwood K J, Eberhard M O. Effective stiffness of reinforced

concrete columns. ACI Structural Journal, 2009, 106(4)

54. Lee H S, Noguchi T, Tomosawa F. Evaluation of the bond properties between concrete and reinforcement as a function of the degree of reinforcement corrosion. Cement and Concrete Research, 2002, 32(8): 1313–1318
55. Ibarra L F, Medina R A, Krawinkler H. Hysteretic models that incorporate strength and stiffness deterioration. Earthquake Engineering & Structural Dynamics, 2005, 34(12): 1489–1511
56. Lignos D G, Krawinkler H. Deterioration modeling of steel components in support of collapse prediction of steel moment frames under earthquake loading. Journal of Structural Engineering, 2011, 137(11): 1291–1302
57. Xu B, Wang X, Yang C S W, Li Y. Probabilistic curvature limit states of corroded circular RC bridge columns: Data-driven models and application to lifetime seismic fragility analyses. Earthquake Spectra, 2024, 40(4): 2805–2835
58. Shamsabadi A, Khalili-Tehrani P, Stewart J P, Taciroglu E. Validated simulation models for lateral response of bridge abutments with typical backfills. Journal of Bridge Engineering, 2010, 15(3): 302–311
59. Muthukumar S, DesRoches R. A Hertz contact model with non-linear damping for pounding simulation. Earthquake Engineering & Structural Dynamics, 2006, 35(7): 811–828
60. Schoettler M, Restrepo J, Guerrini G, Duck D E, Carrea F A. A Full-scale, single-column bridge bent tested by shake-table excitation. PEER Report, 2015, 2: 1–122
61. Henry L, Mahin SA. Study of Buckling Longitudinal Bars in Reinforced Concrete Bridge Columns. Report to the California Department of Transportation. 1999
62. Kunnath S K. El-Bahy A, Taylor A W, Stone W C. Cumulative seismic damage of reinforced concrete bridge piers. Cumulative Seismic Damage of Reinforced Concrete Bridge Piers, 1997: 120–120
63. Lee H S, Kage T, Noguchi T, Tomosawa F. An experimental study on the retrofitting effects of reinforced concrete columns damaged by rebar corrosion strengthened with carbon fiber sheets. Cement and Concrete Research, 2003, 33(4): 563–570
64. Platt J. Probabilistic outputs for support vector machines and comparisons to regularized likelihood methods. Advances in Large Margin Classifiers, 1999, 10(3): 61–74
65. Baker J W. Efficient analytical fragility function fitting using dynamic structural analysis. Earthquake Spectra, 2015, 31(1): 579–599
66. Altekruse J M, Powers P M. Data release for PGV data for the 2018 National Seismic Hazard Model for the conterminous United States. US Geological Survey (USGS) Data Release, 2021: 1055